Addis Ababa University

Addis Ababa Institute of Technology

School of Mechanical & Industrial Engineering

Analysis of Fatigue Crack Propagation and Life Estimation of Pelton Turbine Bucket by Finite Element Method

A Thesis Submitted to the School of Graduate Studies of Addis Ababa Institute of Technology, Addis Ababa University in partial fulfillment for the Degree of Master of Science in Mechanical Engineering (Mechanical Design Stream)

By

Tadele Libay

Advisor: Mulugeta Habtemariam (Ph.D)

November, 2020

Addis Ababa, Ethiopia

ADDIS ABABA UNIVERSITY

SCHOOL OF GRADUATE STUDIES

ADDIS ABABA INSTITUTE OF TECHNOLOGY

SCHOOL OF MECHANICAL & INDUSTRIAL ENGINEERING

Analysis of Fatigue Crack Propagation and Life Estimation of Pelton Turbine Bucket by Finite Element Method

By:

Tadele Libay

Approved By Board of Examiners

Mulugeta Habtemariam (Ph.D.)	_____
Advisor	Signature
Behailu Mamo (Ph.D. Candidate)	_____
Internal Examiner	Signature
Samuel Tesfaye (Ph.D.)	_____
External Examiner	Signature

Declaration

I hereby declare that this thesis work is my original work, has not been presented for a degree in this or any other universities, and all sources of materials used for the thesis work have been fully acknowledged.

Tadele Libay Aligaz _____

Name Signature

Place: Addis Ababa

_____

Date of Submission

This thesis has been submitted for examination with my approval as a university Advisor.

1. Mulugeta Habtemariam (Ph.D.) _____

Advisor Signature

Abstract

The Pelton turbine bucket is subjected to different loads under the turbine operating conditions of high rotational speed. One of the most catastrophic failures that could occur in a Pelton turbine is the fracture of the bucket, where the hydraulic jet force is at its maximum and applied for various cycles. The continual application of this cyclic load will result in nucleation and then fatigue crack propagation. This failure of Pelton turbine bucket has a great influence on durability of the turbine.

The aim of this thesis is to analyze fatigue crack propagation and estimating the life of Pelton turbine bucket. To do this, a governing equation for crack propagation and life estimation was derived and a Pelton turbine bucket was designed.

The three-dimensional model of Pelton turbine bucket was modeled by commercial software SOLIDWORKS. The modeled bucket was then imported to ANSYS 19 workbench. Finite Element analysis was done after meshing, boundary conditions and applying load. Then, static stress analysis and fatigue crack propagation of the turbine bucket was investigated using stress intensity factors.

The stress-intensity factor was evaluated for each increment of crack depth and it was related with fatigue crack growth rate. The fatigue crack life was then calculated for each crack increment. As the result obtained, analysis of fatigue crack propagation and life estimation of the bucket are discussed. And few recommendations are made for the future study.

Key Words: Pelton turbine, Kinetic Energy, Potential Energy, Dynamic Loading, J-Integral, Stress Intensity Factor, Fatigue, Crack Propagation, Fatigue Life.

Table of Contents

Acknowledgments

This thesis would have been a distant reality if not for the help and encouragement from various people.

I take immense pleasure in thanking my advisor Mulugeta Habtemariam (Ph.D.) for his constant encouragement, generous technical and personal support. His guidance and advice have helped me throughout the research and writing for this thesis. He truly exemplifies the merit of technical excellence and academic wisdom. Without his great guidance, this work would never been finished.

I would like to extend my special thanks to Behailu Mamo (Ph.D. Candidate) and all staff members of School of Mechanical and Industrial Engineering for their kind help and cooperation in various ways during this thesis work.

Finally, yet importantly, Thanks to my family and friends for their help and wishes for the successful completion of this project.

Thank GOD!!!

List of Figures

List of Tables

Chapter One

1 Background

1.1 Introduction

Hydropower is currently the most important renewable source of the world's electricity supply. Continued exploitation of this resource is a response to the world's demand for energy. Environmental legislation such as the Kyoto Protocol is putting increasing pressure on all governments to generate clean and green energy from sustainable sources [1].

Hydraulic turbines exploiting the energy of water in dams make an indispensable contribution to the generation of electricity worldwide. The advantages of hydroelectric plants over fossil fuel plants are a higher lifetime, an efficiency rate twice as high and cheaper costs for maintenance and service [2].

Turbines are used for hydropower generation. There are two types of hydraulic turbines, the first one is impulse and the other one is reaction type turbines. Impulse turbines work based on the principle of momentum; while in the reaction type turbines, the flow is fully pressurized and it works according to the principle of conservation of angular momentum. The potential energy of fluid is converted to kinetic energy. Francis and Kaplan type turbines are examples of reaction turbines and Pelton turbine is an example of impulse turbines [3].

The Pelton turbine as shown in figure 1 is one of the most efficient types of hydraulic turbines; it is a cross-sectional flow turbo motor machine with partial admission and action. It consists of a wheel (impeller or rotor) outfitted with buckets in its periphery, which are specially designed to exploit large low flow hydraulic jumps. Hydroelectric plants outfitted with these types of turbines generally have a large pipe called a pressure gallery to transport the fluid from great heights, often more than 200 m. At the end of the pressure gallery, water is provided to the turbine through one or several needle valves, called injectors, which are nozzle shaped to increase the speed of the flow impact upon the buckets. The nozzle launches the water jet directly

against a series of bucket-shaped paddles mounted around the outer border of the runner. The water provides a driving force on the buckets, exchanging kinetic energy with the wheel by virtue of its change in the amount of movement [4].

Figure 1. Pelton Turbine [5].

In the conversion of hydraulic power to mechanical power, Pelton turbine can be used effectively over a relatively wide range head and flow rate when compared to other turbine categories and is suitable for many medium and high heads. However, it can also be used for small heads. The blade of Pelton turbine bucket plays the indispensable role. And it is the major part of the Pelton turbine that greatly influences the efficiency of the turbine. For this reason, this thesis will target on Pelton turbine bucket.

Causes of Damages of Pelton Turbine Bucket

The Pelton turbine bucket (blade) is subjected to different loads under the turbine operating conditions of high rotational speed. Analysis of water flow over the turbine surface initiates stresses on turbine blades and to other components. Turbine materials which are subjected to repeated hydraulic stresses may result into material failure due to fatigue [6].

Defects of a small size rarely occur in a new turbine. Such defects will be detected by a leakage or rupture during the pressure test, which is a very important type of tests at the end of the manufacture. Smaller defects in a new turbine may however, grow to critical size during life time due to crack propagation caused by a certain number of load cycles [7].

1.2 Statement of the Problem

Pelton turbine buckets are subjected to a combination of stresses caused by centrifugal force and water jet cyclic loads. The centrifugal force is induced by the fast rotating body and is related to the runner speed and mass [9]. These loads can possibly influence the turbine performance and durability.

Problems concerning hydraulic turbines are caused mainly by cavitation, sand erosion, material defects and fatigue [7]. But, A case study from Norway [11] shows that a Pelton turbine bucket was fractured from its root as it is shown in the figure below. The cause of crack was fatigue (in the form of corrosion) due to alternating stresses on the lugs. The turbine components which are subjected to repeated alternating or cyclic stress below the normal yield strength fail progressively by cracking, [6]. One of the principal failures and perhaps the most catastrophic failure that could occur in a Pelton turbine is the separation of the bucket from its base at the root, where the bending stress product of the jet force is at its maximum [4].

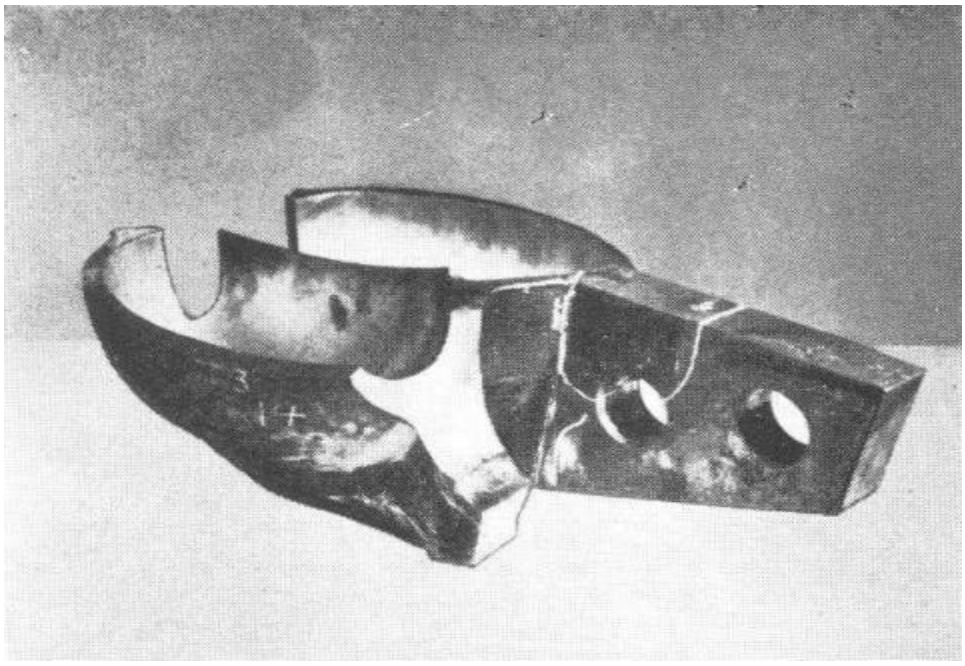

Figure 2: Bucket fracture discovered January 1952 [11].

This type of failure can occur during operation because of defects not detected during maintenance that could cause the disablement of the bucket, destruction of the housing, and in the worst case scenario injury of operators who are near the machine [4]. Once there is a defect on the material, it can be considered as an initiated crack. The initiated crack grows to critical size during life time due to fatigue propagation caused by a certain number of load cycles leads to fracture of the blade [12]. The main focus of this thesis is to understand the behavior and nature of cracks initiated by fatigue loads which have a vital importance in knowing how the cracks propagate and estimating fatigue life of Pelton turbine bucket. This helps in blocking further damages due to the separation of the bucket with its root.

1.3 Objective

1.3.1 General Objective:

The general objective of this thesis is to investigate the fatigue crack propagation and life estimation of Pelton turbine bucket under normal turbine loading condition by finite element method.

1.3.2 Specific Objective:

The specific objectives are:

- To discuss different fracture approach life estimation models.
- To discuss different fatigue crack propagation models.
- To design a micro Pelton turbine bucket.
- To derive a governing equation of kinetic energy of a point in a Pelton turbine bucket.
- To derive a governing equation of potential energy of a point in Pelton turbine un-cracked bucket.
- To derive the equation of motion of Pelton turbine bucket.
- To derive a governing equation of fatigue crack propagation in Pelton cracked turbine bucket.

1.4 Research Methods and Methodology

The methods and methodologies employed to achieve the above objective are:

a) Literature Review

Literature review of relevant material on different methods of fatigue crack propagation and life estimations model will be done. The review will be based on literatures available from electronic media, journals, and books. Besides, secondary data, from previous related research studies, existing statistical data, etc. will be used.

b) Data Collection

The geometrical specifications and the loading conditions data of the Pelton turbine bucket will be analyzed by designing a micro Pelton turbine with the help of a standard design manual.

c) Modeling and Simulation of Pelton Turbine Bucket

Having modeled the 3D model of the bucket using Solid Work software, the Finite Element Method Simulation will be performed using ANSYS 19 Workbench software.

d) Results, Discussion, Conclusion, Recommendation and Future work

Discussion and conclusion will be drawn based on the analysis done on the method and recommendations will be given after concluding the result. Finally; based on the limitations and scope of the thesis, future work will be forwarded for further studies.

1.5 Scope and Limitations

This thesis is intended to analyze fatigue crack propagation and life estimations of Pelton turbine bucket. The cause of crack initiation is due to corrosion and propagation of the crack is due to the applied jet force and centrifugal effect. Since the experimental method is quite expensive to perform fatigue crack propagation and since the set ups are not affordable, this thesis paper is limited to finite element methods.

Even though the bucket is subjected to other environmental loading conditions like corrosion, only the effect of water jet and centrifugal force is taken into consideration and the initiated crack on

the bucket is considered to be a defect because fatigue load. Due to the wideness of research area, the following environmental loading conditions are not addressed in this paper.

- corrosion
- Vibration of the bucket.
- Erosion problems,
- Wear problem,
- Cavitations,
- Thermal load/ creep effect and Surface finish of the material, etc...

1.6 Significance of the Study

The outcome of this research will contribute to the body of knowledge in fracture mechanics in general and specifically in fatigue crack propagation studies. The outcome of this research will benefit potential technicians who design, manufacture and maintain hydroelectric power plants operating with Pelton turbine buckets. The outcome of this research will contribute to the fatigue crack propagation property of Pelton turbine bucket. The outcome of this research will contribute to estimation of fatigue life of Pelton turbine bucket once a crack initiated.

As the experimental method is quite expensive, modeling and simulating using FEM analysis software can reduce the cost and the required result can be found with a short period of time.

1.7 Organization of the Thesis

The first chapter of this thesis introduces the background of the problem by identifying causes for failure of turbine in general and Pelton turbine bucket specifically. Reviewing literatures of previous researches have been done on the important parameters that will be used throughout the thesis. The second chapter deals with the basic concepts of fatigue crack propagation and fracture life estimation models. In the third chapter, derivation of a governing equation of fatigue crack propagation and life estimation is done specifically for Pelton turbine bucket. It also describes the fluid dynamics, solid mechanics and Hamilton's equation of motion.

The fourth chapter introduces the steps used in ANSYS Workbench software for the analysis of required result. The modeling, mesh generation, loading and boundary conditions are briefly discussed.

The fifth chapter discusses the results obtained from ANSYS Workbench software. With increment of crack length, different parameters were calculated and their values are tabulated in tables and different relations are shown with figures.

The sixth chapter discusses conclusions drawn from the results and recommendations for further research are also given.

Chapter Two

2 Literature Review

2.1 Introduction

The huge importance of hydroelectric power plants has been an incentive for conducting various researches from different perspectives to fulfill the growth of industry all over the world. The eventual sophistication of science and technology permitted researchers to focus on the design, failure analysis, and development of better material and processes that could maximize the efficiency of the hydropower turbines.

However, the literature on the Pelton turbine bucket design available is scarce. This might be due to the competitive nature of the hydropower industry and the resulting secrecy in design methods and innovations. Pelton Turbine Bucket.

Reiner Mack, [13] described the history of Pelton turbines as they belong to the family of free jet turbines. Pelton turbines were invented in 1880 by the gold miner Lester Pelton, the design was then refined and optimized over time. The basic principle, however, is still the same. A nozzle is mounted at the end of the pressure line, converting the potential energy of the water into kinetic energy by forming a water jet. The jet is directed to the runner buckets. After the impact, the water leaves the bucket in the opposite direction of the free jet. The rotational energy is then transferred through the shaft to electrical energy using a generator.

Sonendra, N. Agarwal and T.S.Deshmuk, [14] have made an attempt to analyze the stress developed on the surface of the Pelton bucket using Mechanical APDL. The geometric modeling of this blade (bucket) has been done using CATIA software for a 50 m head and stress analysis had been done in Mechanical APDL. They have also done the stress analysis considering bucket as a cantilever element fixed to the disc at one end with the force of jet applied at the splitter. The structural stress analysis has been done for flow rates ranging from 100 lit/sec to 150 lit/sec and speed ranging from 700 rpm to 900 rpm. It is observed that 1st principal stress is higher than 2nd principal stress and 3rd principal stress. The Von-Mises stress decreases as the rotational speed of the Pelton turbine increases.

In Hydroplan UK, [9] It is envisaged that hydraulic performance will improve due to greater control over the bucket surface geometry and finish. They also showed that the problem with Pelton turbine blade has been cyclic fatigue and corrosion exacerbating stress concentrations around the bolt leading to premature failure.

The cyclic load is applied each time the bucket meets the jet. On high-speed multi-jet runners, each bucket can undergo as much as 5 x 1010 repetitive cycles over its lifetime. Therefore, in the design process of Pelton runner susceptibility to fatigue failure must be a major consideration.

2.3 Fatigue Crack Propagation, Equations and Laws of Fatigue Crack Propagation

In engineering, most of problems and disasters are caused by cracking of structures. This have resulted many catastrophes and financial losses. In 1978, the annual cost of fracture in the U.S.A was estimated to be $119 billion which was 4% of the national product. If the current technology was employed, the cost could have been reduced to by quarter [12].

Fatigue in engineering structures is the loss of structural integrity over time due to the repeated or continuous application of stress. The response of the structure to constant stress is called ‘static fatigue’; however, the term fatigue is more generally associated with cyclic stressing. The fatigue phenomenon is common to most engineering materials and it has been estimated that 90% of all the engineering failures occur due to fatigue [10]. This can occur after thousands or millions of load cycles, indicating that the material weakens or experiences fatigue damage due to the repeated loads [15].

A most common distinction in fatigue is between high cycle fatigue (HCF) and low cycle fatigue (LCF). HCF considers events that may occur millions of times in the life of any engineering structure, with a predominantly elastic response. Low cycle fatigue may involve thousands of events before failure but it is associated with more widespread plasticity. There are three main approaches that are commonly used to analyze fatigue life in engineering structure. These are the fatigue life approach (SN approach), the strain life approach, and the fatigue cracks growth approach (FCG approach). The stress life and the strain life approaches are associated with the safe-design philosophy, in which a component is considered to be flaw-free. In the fatigue crack

growth rate approach, an initial flaw distribution is assumed (since it is based on fracture mechanics principle) and knowledge of the conditions and rate at which these cracks grow [10].

Many fatigue crack propagation (FCP) laws and governing equations have been derived both theoretically and experimentally. Recent reviews of FCP equations have described these various theories; only a few, demonstrating the different approaches taken to FCP, will be discussed.

2.3.1 Fatigue Crack Growth Rate Using Energy Release Rate

During crack propagation and fracture, two different surfaces are formed. the energy of original system will change. It will dissipate in the form of heat or remains constant. Griffith related the potential energy and work required to form a crack in equation (1) [12].

$$\frac{dE}{dA} = \frac{dE_p}{dA} + \frac{dW_s}{dA} = 0 \qquad \text{..... (1)}$$

$$-\frac{dE_p}{dA} = \frac{dW_s}{dA}$$

Where E is the total energy, E_p Potential energy from internal strain and external force, W_s is work required to create two new surfaces and dA is increase in crack area.

equation (1) was then improved by Irwin who defined the change in potential energy due to the crack area as the energy release rate which is given by equation (2):

$$G = -\frac{dE_p}{dA} \qquad \text{..... (2)}$$

J. Rice obtained a path independent contour integral, the J-integral, after his first-name Jim, who describes the energy release rate in Linear Elastic Fracture Mechanics, and similar the J-integral which is: $J = G$

$$J = \int_{\Gamma} \left(Udy - T_i \frac{\partial u_i}{\partial x} dS \right) \text{..... (3)}$$

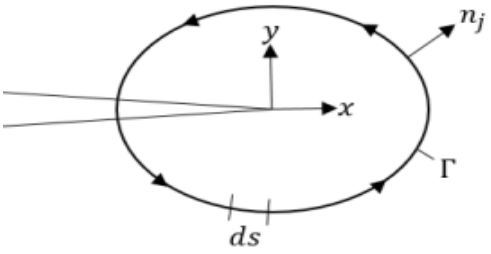

Figure 3:contour around the tip of the crack [16]

Where: $U = \vec{\sigma}_{ij}\varepsilon_{ij}$ is the strain energy density,

$T_i = \vec{\sigma}_{ij}n_j$ is the traction vector,

G is an arbitrary contour around the tip of the crack,

n is the unit vector normal to G

$\vec{\sigma}_{ij}, \varepsilon_{ij}$, and *u* are the stress, strain, and displacement fields, respectively

2.3.2 Fatigue Crack Growth Using Stress Intensity Factor

In order to estimate the lifetime of a structure subjected to a load-case, research has shown a relationship between crack propagation and a number of load cycles called fatigue crack growth rate. For constant amplitude loading, the crack growth rate can be described by followed relationships [12].

$$\frac{da}{dN} = f_1(R, \Delta K) \qquad \text{..... (4)}$$

Where, ΔK is Range in stress intensity, R is Mean stress effect or R-ratio, $\frac{da}{dN}$ is crack growth per cycle.

$$\Delta K = K_{\max} - K_{\min} \qquad R = \frac{K_{\min}}{K_{\max}}$$

J-Integral can also be applied to fatigue accompanied by large-scale yielding; they have assumed a growth law of the form [12].

$$\frac{da}{dN} = f_2(R, \Delta J) \quad (5)$$

Where, ΔJ is a contour integral for cyclic loading. This method can be used for a variety of load types and it is s equal to the energy release rate J=G.

Fatigue crack growth for constant amplitude can be described by the fatigue crack growth rate, da/dN, and stress intensity range ΔK as shown in the sigmoidal curve below.

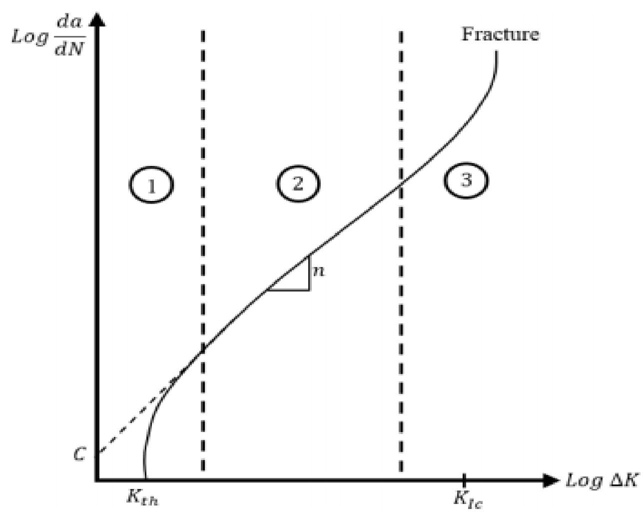

Figure 4: Fatigue crack propagation behaviour[12].

Where K_{th} is a Threshold value which the minimum value of ΔK for crack propagation, K_{IC} is Fracture toughness, the maximum value of ΔK for fracture, $n = m$ is slope of the fatigue crack growth curve in region 2 and C is an intercept of sigmoidal curve in region 2. The material parameters C and m are estimated form experimental testing.

The crack starts to growth at a given threshold value, that is minimum value of the stress intensity factor where the crack start propagates, this is defined as region 1. The crack continues

to propagate in a linear way with increase in stress intensity and crack growth, this step is called region 2. The final end of the crack propagation is fracture where the stress intensity reach the fracture toughness value and a corresponding crack growth value that leads to fracture of the system, this region define the region 3 [12 , 16].

The fatigue crack propagation analysis and life estimation can be done by different models. Here, four different models are listed in the following table.

Table 1: Crack growth models with corresponding regions[16].

Model	Region 1 (K_{th})	Region 2	Region 3 (K_{IC})	Mean Stress Effect (R)
Paris		X		
Forman		X	X	X
NASGROW	X	X	X	X

The Life time can be calculated by arranging the terms in the respective equation from equation (1), (2) and (3) which results:

Paris: $$N = \int \frac{da}{C(\Delta K)^m} \quad \text{..... (6)}$$

Forman: $$N = \int \frac{[(1-R)K_{IC} - \Delta K]da}{C\Delta K^m} \quad \text{..... (7)}$$

NASGROW: $$N = \int \frac{\left(1-\frac{K_{\max}}{K_{IC}}\right)^q da}{C\left[\left(\frac{1-f}{1-R}\right)\Delta K\right]^m \left(1-\frac{K_{th}}{\Delta K}\right)^p} \quad \text{..... (8)}$$

Since it is simple and convenient to use, Paris model will be used for life estimation.

2.3.3 Modes of Fracture

In cracked structures, the stress field near crack-tips may be one of the three modes of fracture as can be seen in the figure below. These modes of fractures are categories as:

Mode I (Tension, opening): In this mode, tensile forces load the body such that the crack surfaces are pulled apart. The deformations are then symmetric. This mode can be demonstrated by figure 5 [17].

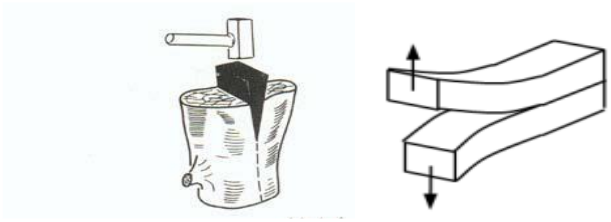

Figure 5. Mode I Opening or splitting

Mode II (In-plane Shear, Sliding): In this mode, the body is loaded by shear force parallel to the crack surfaces, which slide over each other. Figure 6 can demonstrate mode II [17].

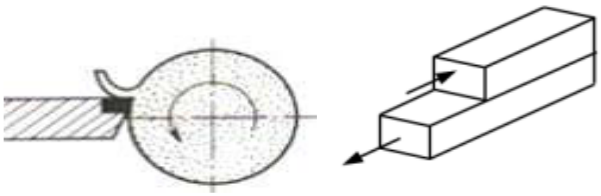

Figure 6. Mode II Shearing or sliding

Mode III (out-of-plane-Shear, Tearing): In this mode, the body is loaded by shear forces parallel to the crack surfaces and the crack surfaces slide over each other Tearing of a paper with a scissors can describe this mode as shown in figure 7 [17].

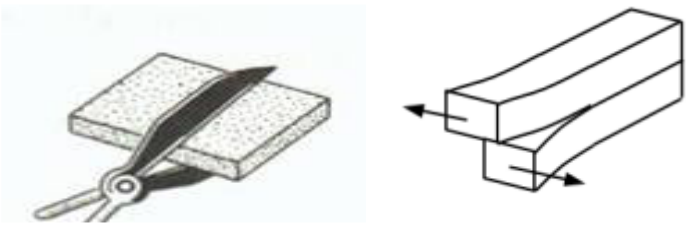

Figure 7. Mode III Tearing

2.3.4 Determination of Crack Location

Arne Kjølle, [7] emphasized that particular attention should be paid to the bucket. If minor defects have been formed, it was recommended to be removed by grinding and polishing according to advice from the manufacturer. The complex shape of the runner buckets makes it difficult to detect defects just below the surface of the bucket. These defects may penetrate up to the surface of the bucket during the first operation time period.

In their research of fatigue life time estimation, Meet Chapani and Bhairav Thakkar, [18] introduced a semi-elliptical crack with a maximum radius of 4mm and a minimum radius of 0.5 mm. Crack meshed with fine 10 nodded tetrahedron elements. Then, they located this crack at maximum equivalent Von-misses stress. They used Goodman's theory to determine the damage and the remaining life of the blade in terms of a number of load cycles. Finally, the fatigue life was determined as a function of the thickness and initial crack length.

Andrea Carpinteri and his team [19] analyzed fracture based fatigue analysis of weld joints. Considering the specimen to be analyzed as a T-Joint or cantilever beam, they located an assumed elliptical crack at the joint (weld) of the specimen and analyzed the stress intensity factor for examining crack propagation.

A.B. Winterbottom, [11] have studied a failure analysis of corrosion fatigue fracture on a bolted Pelton turbine bucket. He inspected a fractured bucket and studied where the crack initiated and propagated. As shown in figure 2, the left lug of the bucket is fractured and above the bolt hole of the right lug, a crack is initiated. Having examined the cracks, he concluded that the crack initiated at the stem of the bucket below the bolt hole.

It’s a fact that the crack propagates with a tensile load. But, the regions on the bucket are subjected to either a compressive or tensile load. Depending on the type of load they are subjected to, the surfaces are either tensile or compressive. From figure 2, the crack could be initiated either at the lower tensile region of the bolt hole or at the upper tensile region on the stem.

For this thesis, the crack is initiated at the upper top tensile region of the stem as it’s discussed in the succeeding sections.

2.4 Material selection for Pelton Turbine Bucket

Many types of research have been done to find the most suitable material for hydropower plants. Since the turbines are subjected to different load types with different environmental factors, finding the most optimized material property was one of the challenges that researchers had faced. To alleviate the problem, different materials are used for different parts of the hydropower plant turbine.

Because of their excellent mechanical properties, 13Cr-4Ni steels are generally used for hydro turbines and water pumps. However, these materials are considerably less resistant to erosive wear and get damaged due to the excessive silt content of the water [20].

Particular attention is given to keeping the cost of materials for the fabrication of the Pelton wheel very low. For micro Pelton turbines Grey Cast Iron, E-glass Fiber, AISI 1018 Steel, CA6nm Steel, and Aluminum Alloy (2024-T3) can be used [21 , 22].

From the recommended materials the aluminum alloy has a defined fracture and strength properties. Besides, the cost of the material is cheaper than the others. Therefore, it's selected for this thesis.

The chemical components of Aluminum Alloy (2024-T3) are:

Component	Al	Cr	Cu	Fe	Mg	Mn	Si	Zn	other
Wt.%	90.7-94.7	0.1	3.8-4.9	0.5	1.2-1.8	0.3-0.9	0.5	0.25	4.35

And both the mechanical and physical material properties are depicted on Table 2.

Table 2: Material properties of 2024-T3[23].

Properties	Values
Density	2780 kg/m^3
Tensile Strength, Ultimate	485 MPa
Tensile Strength, Yield	345 MPa
Elongation at Break	18.00%
Modulus of Elasticity	73.1 GPa
Notched Tensile Strength	379 MPa
Poisson's Ratio	0.33
Fatigue Strength	138 MPa
Plain - Strain Fracture Toughness (K_{IC})	44 $MPa\sqrt{m}$
Threshold Value (ΔK_{th})	1.7 MPa$\sqrt{m}$

Shear Modulus	44.0 GPa
Shear Strength	760 MPa

Having surveyed the literature; in this thesis, the initiated crack will be located in the tensile region of the bucket. Considering the stem of the bucket as a cantilever beam, SIF and J-integral will be used for the analysis of fatigue crack propagation and the life will be estimated using Paris's law and the material used is Aluminum Alloy (2024-T3).

Chapter Three

3 Derivation on Equations of Motion

1.1 Introduction

In this study, to determine the governing equation of motion for the rotating Pelton turbine bucket that exposed to crack, simple approaches are applied. First, the micro Pelton bucket is designed and a governing equation for water jet is derived. Second, a governing equation for the fluid dynamics of the water jet is derived. Third, a governing equation for the rotating Pelton turbine bucket without and with a crack is analyzed considering the stem of the rotating Pelton turbine bucket as a cantilever beam, which will have an energy transformation between Kinetic, potential, and strain energy due to its high angular rotation created by water jet impact. Since the rotation of the bucket is created by fluid motion, the governing equation encompasses both fluid mechanics and solid mechanics.

Stresses on the stem of the bucket are caused by two load cases that can cause the bucket to break off [21].

i. Fatigue load- caused by bending stress on the stem due to the water hitting the bucket every time it passes a nozzle.
ii. Runaway- this occurs when the external load is removed from the turbine and the runner accelerates to a high speed. This produces a large centrifugal force in the buckets, which can snap the stem of the bucket.

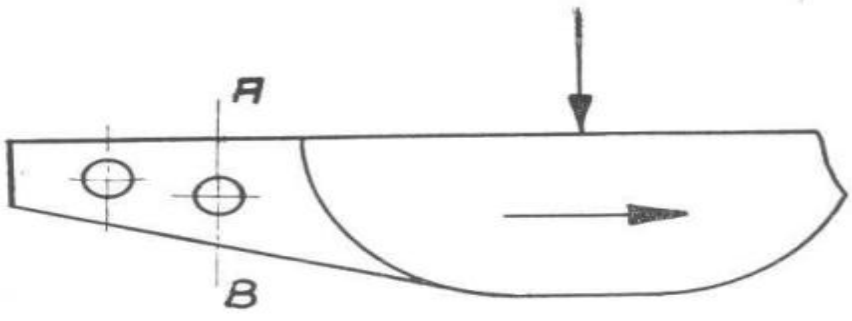

Figure 8: relative positions of resultant jet and centrifugal forces as well as fixing bolts.[11]

1.2 Design Specification of the Model Micro Pelton Wheel Turbine

Taking the loading conditions data of design manual [21] the water falls from a net head (H_n) of 120 m at a flow rate (Q) of 144l/s. The Pelton wheel is expected to run at a certain specific speed (Ns) to transfer torque (T) to the electric generator to produce power (P) whose main technical specifications are detailed in Table 3.

Table 3. Pelton turbine technical specifications [21]

Flow rate (l/s)	144
Net Head (m)	120
No of Jets	2
Runner PCD (m)	400
Jet Diameter (mm)	44.1
Turbine Speed (rpm)	1032
Gear Ratio	1.45

Therefore, as the manual recommends, all the other design specifications are evaluated from the above main specification of the turbine. The geometric specifications are mainly dependent on the pitch circle diameter (PCD) of the turbine and their relation can be shown in the figure below. Where the given dimensions are the percent of PCD.

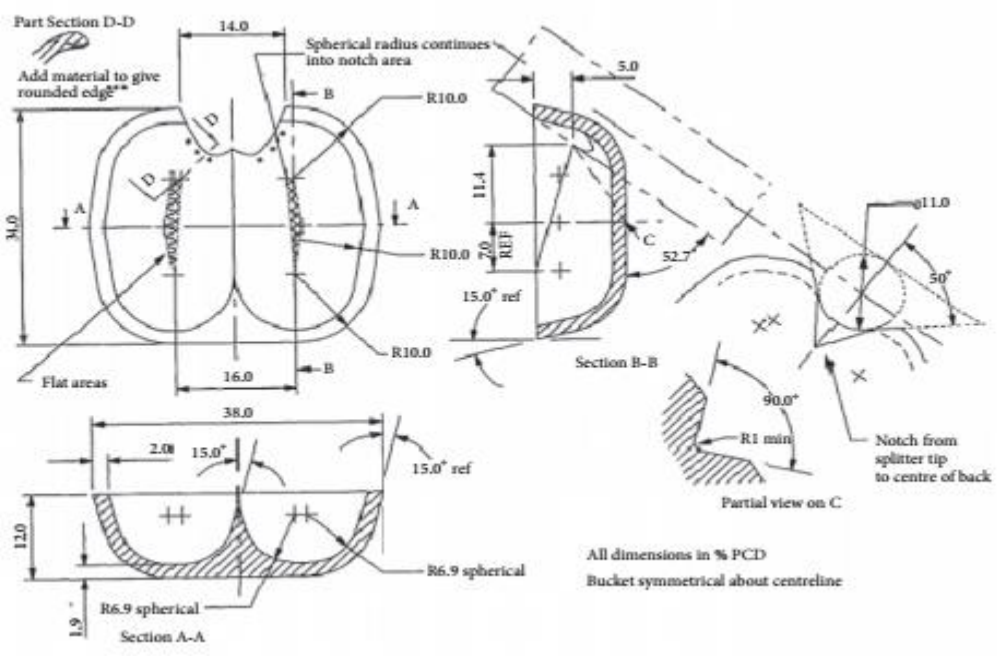

Figure 9: Geometry of Pelton Bucket. All dimensions are in % of PCD [21]

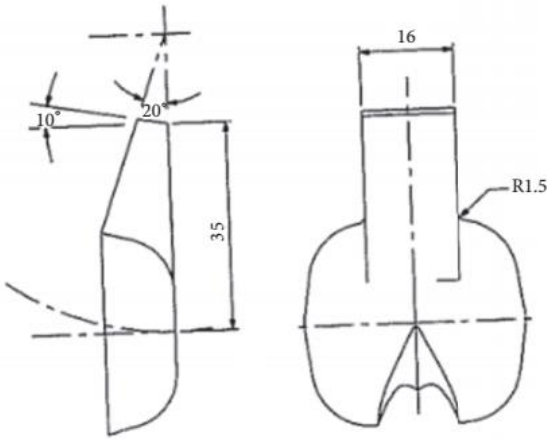

Figure 10: A basic bucket stem design for bolted fixing. All dimensions are in % of PCD [21]

From figures 9 and 10, the following geometrical specifications of the turbine bucket are calculated. Their values are tabulated in table 4. The bolt holes are designed in such a way that the bolts can withstand the loads applied to the turbine bucket. Two bolts are used with diameters of 12mm and 10 mm. The bolt holes dimensions are shown in figure 12.

Table 4: baseline bucket dimensions

Parameters, Formula [21]	Calculation	Value	Unit
Height of bucket, h = 34%D	h = 0.34 × 400	136	mm
Cavity length: h_1 = 5.6%D	$h1$ = (0.056) × 400	22.4	mm
Length to impact point: h_2 = 11.4%D	$h2$ = 0.114 × 400	45.6	mm
Width of bucket opening, a=14%D	a=0.14×400	56	mm
Bucket thickness: t_1=1.9%D	0.019×400	7.6	mm
Depth of the bucket, t=12%D	t=0.12×400	48	mm
Width of the bucket, b=0.38%D	b=0.38×400	152	mm

Using the geometrical specifications depicted in table 4, the three-dimensional Pelton turbine bucket is modeled using Solidwork 2016. And it is shown in the figure below.

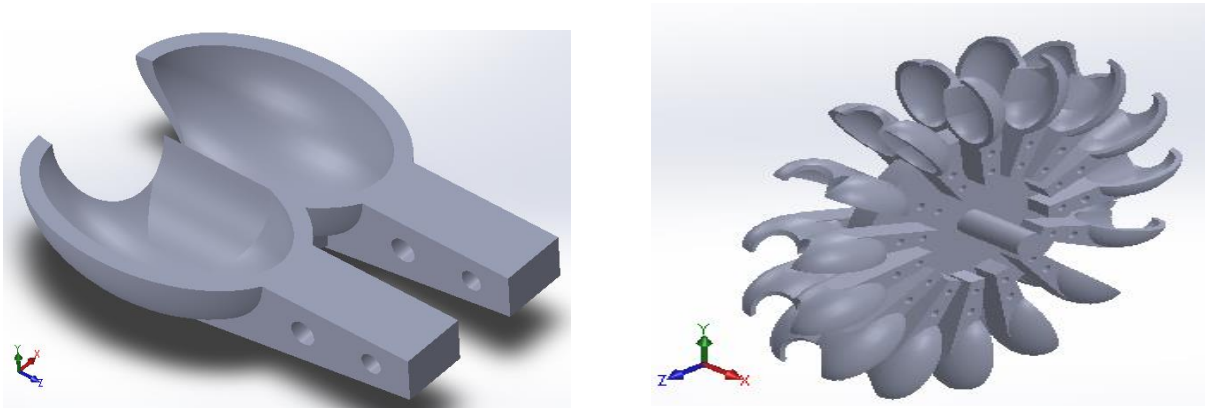

(a) (b)

Figure 11: 3D model of Pelton turbine, (a) bucket and (b) 3D view of the runner

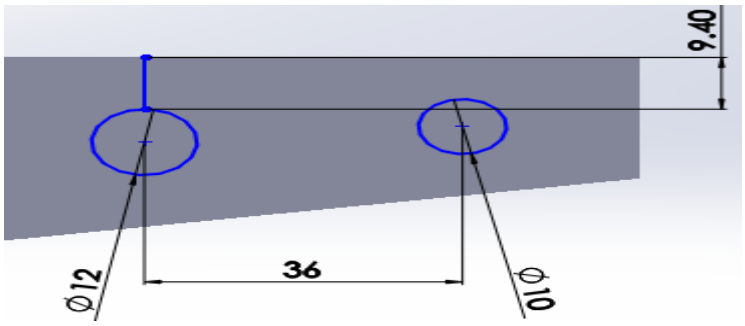

Figure 12: Bolt holes dimensions (all are in mm)

1.3 Fundamental Equations of Fluid Mechanics

When a water jet passes through the turbine surfaces, a reciprocal action takes place. The particle deviates from its initial direction; the Momentum change induces a pressure on the blade surfaces and causes the rotation of the latter, thereby generating a torque upon the turbine shaft. The torque is expressed as [24]:

$$\vec{T} = \frac{d}{dt}(\vec{r} \times m.\vec{c}) \quad \text{..} (14)$$

Where, $\vec{T}$ = the torque exerted on the shaft

$\vec{r}$ = the radius of the turbine runner

$\vec{c}$ = velocity of water jet

Generally, a fluid motion is described by a set of 3 equations; these are (i) conservation of mass, (ii) conservation of Momentum, and (iii) conservation of energy.

3.3.1 Conservation of Mass

Since the total amount of fluid in a control volume V is conserved with density ρ, the mass flow rate can be written as:

$$\frac{d}{dt}\int_V \rho dV = 0 \quad \text{..} (15)$$

Using the Reynolds transport theorem, Eq (15) leads to

$$\int_V \left(\frac{\partial \rho}{\partial t} + \vec{\nabla} \bullet (\rho \vec{c}) \right) dV = 0 \quad \text{..} (16)$$

Since Eq (16) must apply even to an infinitesimal volume of control, one obtains:

$$\frac{\partial \rho}{\partial t} + \vec{\nabla} \bullet (\rho \vec{c}) = 0 \quad \text{..} (17)$$

or

$$\frac{\partial \rho}{\partial t} + \rho \vec{\nabla} \bullet \vec{c} = 0 \quad \text{..... (18)}$$

3.3.2 Conservation of Momentum

In applying Newton's second law of motion to a finite, extended mass of fluid, the external resultant force is equated to the rate of change of resultant momentum which is calculated for a mass of fluid consisting of the same fluid particles Thus,

$$\frac{d}{dt}\int_V \vec{c}\,\rho dV = \int_V \vec{c}\,\rho \vec{F} dV + \int_S \vec{\bar{T}} \bullet \vec{n} dS \quad \text{..... (19)}$$

Where $\vec{F}$ the body force per unit volume acting on the fluid, $\vec{\bar{T}}$ is the stress tensor, *S* is the surface of control enclosing *V*, and $\vec{n}$ is the unit outward normal to the area element dS.

Using the Reynolds transport theorem, Eq. 19 becomes:

$$\int_V \left(\frac{\partial \rho}{\partial t}(\rho \vec{c}) + \vec{\nabla} \bullet (\rho \vec{c} \vec{c}) \right) dV = \int_V \rho \vec{F} dV + \int_S \vec{\bar{T}} \bullet \vec{n} dS \quad \text{..... (20)}$$

Using Green's theorem and Eq (17), Eq (20) becomes:

$$\rho \left(\frac{\partial \vec{c}}{\partial t} + \vec{c} \vec{\nabla} \square \vec{c} \right) = \rho \vec{F} + \vec{\nabla} \square \vec{\bar{T}} \quad \text{..... (21)}$$

The terms of the stress tensor stem from the pressure and the viscous terms, and can be rewritten as:

$$\vec{\bar{T}} = P\vec{\bar{I}} + \mu \vec{c} \otimes \vec{c} \quad \text{..... (22)}$$

The Momentum equation, Eq (21) then becomes the Navier-Stokes equation:

$$\frac{\partial \vec{c}}{\partial t} + \vec{c} \vec{\nabla} \square \vec{c} = \frac{-1}{\rho} \vec{\nabla} P + \mu \nabla^2 \vec{c} + \vec{f} \quad \text{..... (23)}$$

Where, P is the pressure and μ is dynamic viscosity

3.3.3 Conservation of Energy

Considering the energy balance for the fluid in volume *V*, Work is done on this mass of fluid by both body and surface forces, and heat may also be transferred across the surface of control *S*. Some of this work done and heat transferred shows up as an increase in the kinetic energy of the fluid, and the reminder shows up as an increase in the internal energy of the fluid, according to the first law of thermodynamics.

The equation expressing the first law of thermodynamics is then:

$$\frac{d}{dt}\int_V \rho\left(e+\frac{1}{2}\vec{c}^{\,2}+U\right)dV=\frac{dQ}{dt}+\frac{dW}{dt} \quad \ldots\ldots\ldots\ldots\ldots\ldots (24)$$

Where, *e* is the internal energy of the fluid per unit mass, *U* is the potential energy of the fluid in a conservative body- force field $\vec{f}=-\vec{\nabla}U$, Q is the heat transfer to the system, and *W* the work delivery from the system. Using the Reynolds transport theorem, the continuity equation, Eq. 17, and after some algebraic manipulation, the conservation of energy finally becomes:

$$\rho\left(\frac{\partial}{\partial t}\left(e+\frac{1}{2}\vec{c}^{\,2}+U\right)+\vec{c}\vec{\nabla}\left(e+\frac{1}{2}\vec{c}^{\,2}+U\right)\right)=\frac{dQ}{dt}+\frac{dW}{dt} \quad \ldots\ldots\ldots\ldots\ldots (25)$$

The above derived equations govern the fluid dynamics of water jet. The impact of the jet with turbine bucket can be considered as a distributed load in a specific area. Taking the hydraulic pressure as a stress, it will be acted on the bucket of the Pelton turbine repeatedly.

Theoretically, on a Pelton turbine, all the energy available in the flow becomes kinetic energy at atmospheric pressure through a nozzle before the fluid comes in contact with the moving bucket [4].

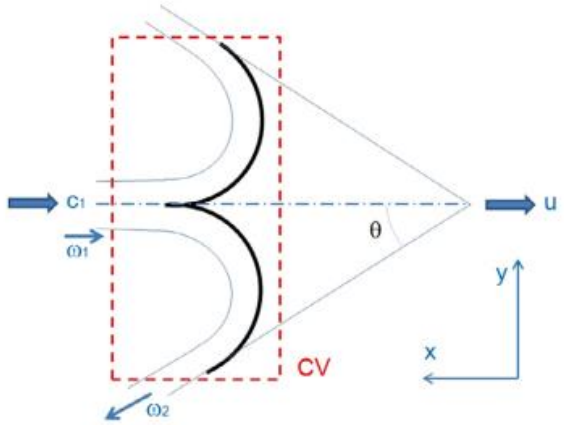

Figure 13: Flow through a bucket [4]

Figure 13 shows that at the bucket entry, absolute C1 and tangential u speeds have the same direction and sense; thereby, it can be written as:

$$\omega_1 = C_1 - u \quad \text{.....} \quad (26)$$

Where ω_1 is the relative speed of entry between the jet speed C_1 and the impeller tangential speed u. At the control volume (CV) output, the direction of the relative speed ω_2 is defined by the output angle h, and we have:

$$\omega_2 = K_m \omega_1 \quad \text{.....} \quad (27)$$

Where, K_m is the denominated bucket coefficient that depends on the thickness of the water layer, surface roughness of the bucket, and type of material. Its value varies between 0.88 and 0.92.

Finally, an expression is obtained for the force of the jet on the bucket:

$$F_{jet} = \rho Q (C_1 - u)(K_m \cos\theta + 1) \quad \text{.....} \quad (28)$$

$$C_1 = C_v \sqrt{2gH_n} \quad \text{.....} \quad (29)$$

Where, ρ is the water density and is equal to 998 kg/m^3 at 20°C, Q is water flow rate, θ is output angle.

Substituting the values on equation (28) results, $F_{jet} = 1813.55N$

For a normal condition the pressure P is given by:

$$P = \frac{F}{A_{jet}} \text{ .... (30)}$$

Where of A_{jet} is area of water jet which is,

$$A_{jet} = \frac{\pi (d_{jet})^2}{4}$$

Substituting the values on equation (30) results, $P = 1.1901\ MPa$

Considering the actual case of last jet impact on the bucket from a nozzle it is a fact that once the jet strikes the splitter, water is distributed throughout the bucket profile. And the distributed water pressure is considered to have equal magnitude on the surface of the bucket. Therefore, the pressure will have two components (Y and Z). They are assumed to be equal. Thus,

$$P_y = P_z = 8.415 \times 10^5\ Pa$$

But besides water jet, the bucket is also subjected to a centrifugal force (Runaway Force). This force can be specified by angular speed of the runner. And it can be expressed as follows.

$$F_{runaway} = m_{bucket} \times R_g \times \omega^2{}_{runaway}$$

$$F_{runaway} = \rho_{bucket} \times V_{bucket} \times R_g \times \left[\frac{2\pi N_{runaway}}{60}\right]^2$$

Where, $N = 37.7\frac{\sqrt{H_n}}{D} = 1033rpm$ and $N_{runaway} = 1.8N = 1860rpm$

$$V_{bucket} = 0.0069D^3 = 4.416 \times 10^{-4} m^3$$

R_g is radius of bucket center of mass.

$$R_g = 0.48D = 0.192m$$

ρ_{bucket} is dependent on the material property of the bucket. In this thesis the material selected is an Aluminum-Alloy and its property is given in Table 4.

Therefore, the runaway force can be taken in terms of runaway speed (angular speed).

$$\omega = \left[\frac{2\pi N_{runaway}}{60}\right] = 195 rad/s$$

1.4 Mechanics of Rotating Pelton Turbine Bucket without a Crack

Due to the applied load of water jet, rotational motion on Pelton turbine bucket will be created. The rotating Pelton turbine bucket can be considered as a cantilever beam where one of its sides is fixed with the turbine disc and the other end is free.

Assuming the bucket as a plate subjected to lateral load or force of the jet and the stem of the bucket as a beam, the displacements, strains and stresses can be calculated using plate theory.

The area of the bucket subjected to the water jet force is irregular surface. Projecting the diameter of the jet and assuming the contact area of the bucket with the jet as a plane, the applied load on that specific area is given by the figure 14.

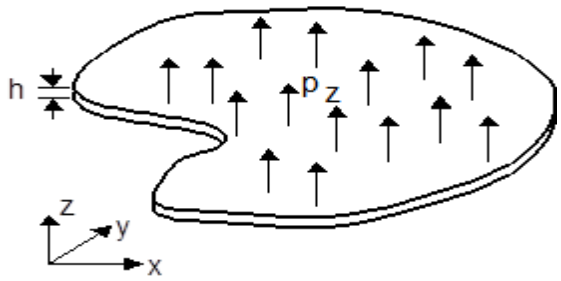

Figure 14. Plate Geometry [25]

1.4.1 Equilibrium Equation

For a two-dimensional plate analysis, it is more convenient to define stress resultants per unit length by integrating only through the thickness. The general stress components acting on an infinitesimal element are shown in the figure 15 and the equations will be written in Cartesian coordinate as follows [25 , 26].

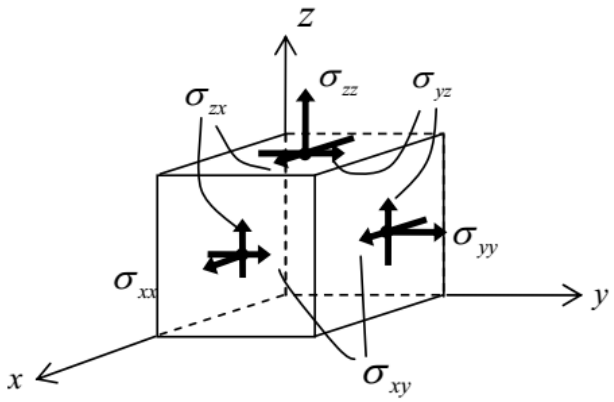

Figure 15. Free Body of Stress Components [25]

The equations of equilibrium neglecting the inertial effect for an infinitesimal element in terms of stresses will be:

$$\frac{\partial \sigma_{xx}}{\partial x}+\frac{\partial \sigma_{yx}}{\partial y}+\frac{\partial \sigma_{zx}}{\partial z}+X=0$$
$$\frac{\partial \sigma_{xy}}{\partial x}+\frac{\partial \sigma_{yy}}{\partial y}+\frac{\partial \sigma_{zy}}{\partial z}+Y=0 \quad \text{..... (32)}$$
$$\frac{\partial \sigma_{xz}}{\partial x}+\frac{\partial \sigma_{yz}}{\partial y}+\frac{\partial \sigma_{zz}}{\partial z}+Z=0$$

Where, X, Y and Z are described as body forces per unit volume.

To make the analysis easier, 8 *stress resultants* (forces and moments per unit length) can be defined by integrating through the thickness (dz) of the plate:

$$N_x = \int_t \sigma_{xx} dz, \quad N_y = \int_t \sigma_{yy} dz, \quad N_{xy} = N_{yx} = \int_t \sigma_{xy} dz$$
$$M_x = -\int_t z\ \sigma_{xx} dz, \quad M_y = -\int_t z\ \sigma_{yy} dz, \quad M_{xy} = M_{yx} = -\int_t z\ \sigma_{xy} dz \quad \ldots\ldots\ldots\ldots\ldots\ldots (33)$$
$$Q_x = -\int_t \sigma_{xz} dz, \quad Q_y = -\int_t \sigma_{yz} dz$$

These force and moment resultants are shown in the figure 16.

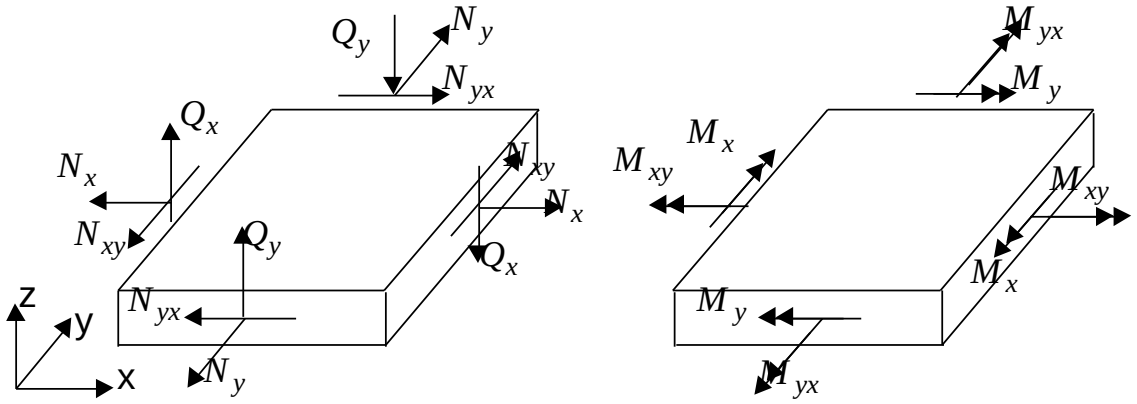

Figure 16. Force and Moment Stress Resultants[25]

Where N_x and N_y are in plane membrane forces per unit length (due to stretching of the plate mid surface), M_x and M_y are bending moments per unit length about the y and x axes, respectively, Q_x and Q_y are transverse shear forces per unit length, N_{xy} is an in-plane shear force per unit length and M_{xy} and M_{yx} are twisting moments per unit length [25 , 26].

Equilibrium of the plate mid-surface in terms of stress resultants is derived using summation of forces and moments in the x, y and z directions. It is assumed that the plate mid-surface is subjected to applied distributed loads p_x, p_y and p_z (force per unit area).

For clarity, let us see the summation of forces only in X-direction as it is shown in figure 17 .

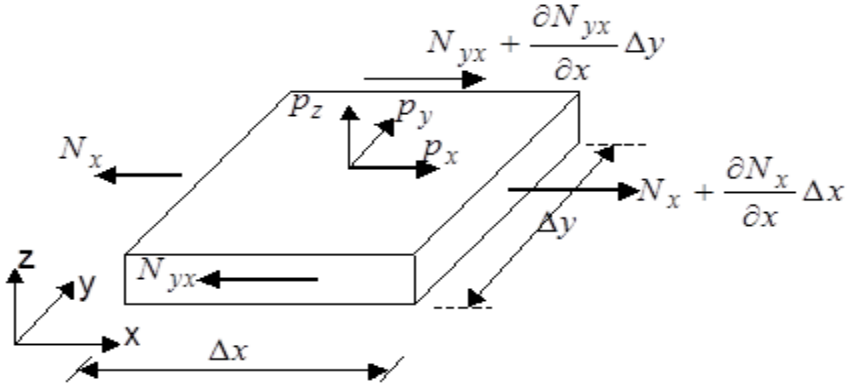

Figure 17. Summation of Forces in X-direction [25]

N_x and N_{yx} can be written as Taylor series in x and y, respectively. Then,

$$0 = \sum F_x = (N_x + \frac{\partial N_x}{\partial x}\Delta x)\Delta y - N_x\Delta y + (N_{yx} + \frac{\partial N_{yx}}{\partial y}\Delta y)\Delta x - N_{yx}\Delta y + p_x\Delta x\Delta y \quad \ldots\ldots\ldots \quad (34)$$

Divide by $\Delta x\Delta y$ and we obtain:

$$\frac{\partial N_x}{\partial x} + \frac{\partial N_{yx}}{\partial y} + p_x = 0 \quad \ldots\ldots\ldots\ldots\ldots\ldots\ldots\ldots\ldots \quad (35)$$

Similarly, we can do force equilibrium in y and z directions, and moment equilibrium about the x and y-axes. Hence, we have 5 equilibrium equations in terms of force and moment stress resultants:

$$\begin{aligned}
&\frac{\partial N_x}{\partial x} + \frac{\partial N_{yx}}{\partial y} + p_x = 0 \\
&\frac{\partial N_{xy}}{\partial x} + \frac{\partial N_y}{\partial y} + p_y = 0 \\
&\frac{\partial Q_x}{\partial x} + \frac{\partial Q_y}{\partial y} - p_z = 0 \\
&\frac{\partial M_x}{\partial x} - \frac{\partial M_{yx}}{\partial y} - Q_x = 0 \\
&\frac{\partial M_{xy}}{\partial x} + \frac{\partial M_y}{\partial y} - Q_y = 0
\end{aligned} \quad \ldots\ldots\ldots\ldots\ldots\ldots\ldots\ldots\ldots\ldots\ldots \quad (36)$$

1.4.2 Compatibility Equation

Assuming that all displacements and strains are small (infinitesimal), strain-displacement equations results in:

$$\varepsilon_{xx} = \frac{\partial u}{\partial x} = \frac{\partial u(x,y,0)}{\partial x} - z\frac{\partial^2 w(x,y,0)}{\partial x^2}$$
$$\varepsilon_{yy} = \frac{\partial v}{\partial y} = \frac{\partial v(x,y,0)}{\partial y} - z\frac{\partial^2 w(x,y,0)}{\partial y^2} \quad \text{..... (37)}$$
$$\varepsilon_{xy} = \frac{\partial u}{\partial y} + \frac{\partial v}{\partial x} = \frac{\partial u(x,y,0)}{\partial y} + \frac{\partial v(x,y,0)}{\partial x} - 2z\frac{\partial^2 w(x,y,0)}{\partial x \partial y}$$

Since all displacements are at the mid-surface and are functions of x and y only, the functional notation of (x,y,0) will be dropped and the above expressions will be rewritten as:

$$\varepsilon_{xx} = \frac{\partial u}{\partial x} = \frac{\partial u}{\partial x} - z\frac{\partial^2 w}{\partial x^2}$$
$$\varepsilon_{yy} = \frac{\partial v}{\partial y} = \frac{\partial v}{\partial y} - z\frac{\partial^2 w}{\partial y^2} \quad \text{..... (38)}$$
$$\varepsilon_{xy} = \frac{\partial u}{\partial y} + \frac{\partial v}{\partial x} = \frac{\partial u}{\partial y} + \frac{\partial v}{\partial x} - 2z\frac{\partial^2 w}{\partial x \partial y}$$

1.4.3 Constitutive Equation

The stresses and strains can be related in the following equation [25].

$$\sigma_{xx} = \frac{E}{1-\nu^2}(\varepsilon_{xx} + \nu\varepsilon_{yy})$$
$$\sigma_{yy} = \frac{E}{1-\nu^2}(\varepsilon_{yy} + \nu\varepsilon_{xx}) \quad \text{..... (39)}$$
$$\sigma_{xy} = G\varepsilon_{xy} = \frac{E}{2(1+\nu)}\varepsilon_{xy}$$

Where E is Young's modulus, G is Shear modulus and ν is Poisson's ratio.

3.4.5 Stress-Displacement Relations

Substituting the compatibility relations into the constitutive relations gives the following stress-displacement relations

$$\sigma_{xx} = \frac{E}{1-\nu^2}\left[\frac{\partial u}{\partial x} + \nu\frac{\partial v}{\partial y} - z\left(\frac{\partial^2 w}{\partial x^2} + \nu\frac{\partial^2 w}{\partial y^2}\right)\right]$$
$$\sigma_{yy} = \frac{E}{1-\nu^2}\left[\frac{\partial v}{\partial y} + \nu\frac{\partial u}{\partial x} - z\left(\frac{\partial^2 w}{\partial y^2} + \nu\frac{\partial^2 w}{\partial x^2}\right)\right] \quad \text{..... (40)}$$
$$\sigma_{xy} = G\varepsilon_{xy} = \frac{E}{2(1+\nu)}\left[\frac{\partial u}{\partial y} + \frac{\partial v}{\partial x} - 2z\frac{\partial^2 w}{\partial x \partial y}\right]$$

Substituting the above equations into the definitions for stress resultants (equilibrium equation) and integrating through the thickness (assuming that u, v and w do not depend on z), yields the following equations:

$$N_x = K\left(\frac{\partial u}{\partial x} + \nu\frac{\partial v}{\partial y}\right) \qquad M_x = D\left(\frac{\partial^2 w}{\partial x^2} + \nu\frac{\partial^2 w}{\partial y^2}\right) \quad \text{..... (41)}$$
$$N_y = K\left(\frac{\partial v}{\partial y} + \nu\frac{\partial u}{\partial x}\right) \qquad M_y = D\left(\frac{\partial^2 w}{\partial y^2} + \nu\frac{\partial^2 w}{\partial x^2}\right)$$
$$N_{xy} = N_{yx} = \frac{1}{2(1+\nu)}K\left(\frac{\partial v}{\partial x} + \nu\frac{\partial u}{\partial y}\right) \quad M_{xy} = -M_{yx} = (1-\nu)D\frac{\partial^2 w}{\partial x \partial y}$$

Now, Q_x and Q_y are obtained by using the last two equilibrium equations.

$$K = \frac{Eh}{(1-\nu^2)}$$
$$D = \frac{Eh^3}{12(1-\nu^2)} \quad \text{..... (42)}$$

Where, K and D in plate theory are the axial and bending stiffness respectively.

3.4.6 Formulation and Solution of the Bucket Equations

We can now develop the differential equations of equilibrium in terms of the displacements u, v and w and the applied loads. Substituting the stress resultant-displacement relations into these two force equilibrium equations results [25 , 26].

$$K\left(\frac{\partial^2 u}{\partial x^2}+\nu\frac{\partial^2 v}{\partial x\partial y}\right)+\frac{K}{2(1-\nu)}\left(\frac{\partial^2 v}{\partial x\partial y}+\frac{\partial^2 u}{\partial y^2}\right)=-p_x$$
$$K\left(\frac{\partial^2 v}{\partial y^2}+\nu\frac{\partial^2 u}{\partial x\partial y}\right)+\frac{K}{2(1-\nu)}\left(\frac{\partial^2 u}{\partial x\partial y}+\frac{\partial^2 v}{\partial x^2}\right)=-p_y \quad \text{..... (43)}$$

Substituting the two moment equilibrium equations into the transverse force equilibrium equation gives:

$$\frac{\partial^2 M_x}{\partial x^2}-\frac{\partial^2 M_{yx}}{\partial x\partial y}+\frac{\partial^2 M_y}{\partial y^2}+\frac{\partial^2 M_{xy}}{\partial x\partial y}=p_z \quad \text{..... (44)}$$

Noting that $M_{xy}=-M_{yx}$, then the above equation may be written as

$$\frac{\partial^2 M_x}{\partial x^2}+2\frac{\partial^2 M_{yx}}{\partial x\partial y}+\frac{\partial^2 M_y}{\partial y^2}=p_z \quad \text{..... (45)}$$

The last equation can be written in terms of the transverse displacement w by substituting for the moment resultants in terms of w. Using the notation (the Laplacian operator)

$$\nabla^2()\equiv\frac{\partial^2()}{\partial x^2}+\frac{\partial^2()}{\partial y^2} \quad \text{..... (46)}$$

We obtain the following equation.

$$\nabla^2(D\nabla^2 w)-(1-\nu)\left(\frac{\partial^2\left(D\frac{\partial^2 w}{\partial y^2}\right)}{\partial x^2}+\frac{\partial^2\left(D\frac{\partial^2 w}{\partial x^2}\right)}{\partial y^2}-2\frac{\partial^2\left(D\frac{\partial^2 w}{\partial x\partial y}\right)}{\partial x\partial y}\right)=p_z \quad \text{.....}$$

(47)

Assuming a constant material properties and thickness for the plate, D will be constant and the terms in the bracket will be zero; and the equation (47) reduces to:

$$D\nabla^4 w = p_z \quad \text{..... (48)}$$

Where, $\nabla^4 w \equiv \frac{\partial^4 w}{\partial x^4} + 2\frac{\partial^4 w}{\partial x^2 \partial y^2} + \frac{\partial^4 w}{\partial y^4}$

Solutions of the above partial differential equations constitute the solution of the plate bending problems. It should be noted that all five equilibrium equations (two in-plane and one transverse force equilibrium equations and the moment equilibrium equation) have been utilized to obtain the three partial differential equations above. The partial differential equations defining the in-plane displacements u and v are coupled. Consistent with small strain theory, the partial differential equation for the transverse displacement w is uncoupled from u and v [25 , 26].

3.5 Kinetic Energy of the Rotating Pelton Turbine Bucket

The kinetic energy of the rotating turbine bucket can be derived by specifying a position of a point anywhere in the bucket.

For a point P anywhere in the bucket, its position vector $\vec{r}$ is [27]:

$$\vec{r} = u_i + v_j + w_k \quad \text{..... (49)}$$

Where u_i, v_j and w_k are the unit vectors in the X, Y and Z directions.

For the angular rotation $\frac{\partial u}{\partial t} = \Omega i$; since there is no bending about the middle surface as it's assumed, the velocity of the turbine runner can be written as:

$$\vec{V} = \frac{dr}{dt} = \left(\frac{\partial u}{\partial t} + v\frac{\partial u}{\partial t} + w\frac{\partial u}{\partial t}\right)i + \left(u\frac{\partial u}{\partial t} - \frac{\partial v}{\partial t} - w\frac{\partial u}{\partial t}\right)j + \left(-u\frac{\partial u}{\partial t} - v\frac{\partial u}{\partial t} + \frac{\partial w}{\partial t}\right)k \quad \text{..... (50)}$$

Where,

$$\frac{di}{dt}=\frac{du}{dt}j-\frac{du}{dt}k \quad , \quad \frac{dj}{dt}=-\frac{du}{dt}i+\frac{du}{dt}k \quad \text{and} \quad \frac{dk}{dt}=\frac{du}{dt}i-\frac{du}{dt}j$$

Then, the general kinetic energy can be expressed as:

$$T=\frac{1}{2}\rho h\int_A \vec{V}\bullet\vec{V}dA \quad \ldots\ldots\ldots\ldots\ldots\ldots\ldots\ldots\ldots\ldots\ldots\ldots\ldots\ldots\ldots\ldots \quad (51)$$

Where, ρ is the mass density of the bucket, h is the thickness, and A is the area of the runner.

Substituting the expression of velocity in equation (51) gives the following equation.

$$T=\frac{1}{2}\rho h\int_A\left[\left(\frac{\partial u}{\partial t}+v\frac{\partial u}{\partial t}+w\frac{\partial u}{\partial t}\right)^2+\left(u\frac{\partial u}{\partial t}-\frac{\partial v}{\partial t}-w\frac{\partial u}{\partial t}\right)^2+\left(-u\frac{\partial u}{\partial t}-v\frac{\partial u}{\partial t}+\frac{\partial w}{\partial t}\right)^2\right]dA \quad \ldots\ldots \quad (52)$$

Where, $\begin{matrix} i.i=1 \\ i.j=0 \\ i.k=0 \end{matrix}$, $\begin{matrix} j.i=0 \\ j.j=1 \\ j.k=0 \end{matrix}$ and $\begin{matrix} k.i=0 \\ k.j=0 \\ k.k=1 \end{matrix}$

Simplifying the above equation gives:

$$T=\frac{1}{2}\rho h\int_A\left\{\left[\left(\frac{\partial u}{\partial t}\right)^2+\left(\frac{\partial v}{\partial t}\right)^2+\left(\frac{\partial w}{\partial t}\right)^2\right]+2\left(\frac{\partial u}{\partial t}\right)^2\left[u^2+v^2+w^2+u(v-w)+v(w+1)+w\right]\right.$$
$$\left.-2\left(\frac{\partial u}{\partial t}\right)\left(\frac{\partial v}{\partial t}\right)(u-w)-2\left(\frac{\partial u}{\partial t}\right)\left(\frac{\partial w}{\partial t}\right)(u+v)\right\}dA \quad . \quad (53)$$

3.6 Potential Energy of the Rotating Pelton Turbine Bucket

Strain energy is a type of potential energy arising from stress and deformation of elastic solids. In an elastic solid, the work of external forces, W, is stored entirely as elastic strain energy, U, within the solid [12 , 28].

Considering the bucket as an elastic body, elastic potential energy of the bucket can be considered to be equal with the strain energy.

$$U = U_o - W_{ex} \quad \text{..... (54)}$$

Where, U is the total internal strain energy, U_o is Strain energy and W_{ex} is Work done due to external force.

Thus, the strain energy U_o, per unit volume for turbine bucket is given by the equation (55):

$$\frac{dU_o}{dV} = \sum \frac{1}{2} \vec{\sigma} \varepsilon \quad \text{..... (55)}$$

Where U_o is Strain energy, $\vec{\sigma}$ is stress, ε is strain and V is the volume of the bucket. For a two-dimensional strain, the strain energy can be expressed as:

$$U_o = \frac{1}{2} \int_V \left(\vec{\sigma}_{xx} \varepsilon_{xx} + \vec{\sigma}_{yy} \varepsilon_{yy} + \vec{\sigma}_{xy} \varepsilon_{xy} \right) dV \quad \text{..... (56)}$$

Integrating equation (56) with respect to dz can give the following equation where A is the area of the bucket.

$$U_o = \frac{1}{2} \int_A \left[\int_{-h/2}^{-h/2} \left(\vec{\sigma}_{xx} \varepsilon_{xx} \right) dz + \int_{-h/2}^{-h/2} \left(\vec{\sigma}_{yy} \varepsilon_{yy} \right) dz + \int_{-h/2}^{-h/2} \left(\vec{\sigma}_{xy} \varepsilon_{xy} \right) dz \right] dA \quad \text{..... (57)}$$

Using equation (33), equation (57) can be rewritten as:

$$U_o = \frac{1}{2} \int_A \left[N_x \varepsilon_{xx} + N_y \varepsilon_{yy} + N_{xy} \varepsilon_{xy} \right] dA \quad \text{..... (58)}$$

Substituting the values of forces N from equation (41), strain ε from equation (38) and the axial stiffness from equation (42) results:

$$U_o = \frac{1}{2}\int_A \left\{ \left\langle \frac{Eh}{(1-\nu^2)}\left(\frac{\partial u}{\partial x}+\nu\frac{\partial v}{\partial y}\right)\left(\frac{\partial u}{\partial x}-z\frac{\partial^2 w}{\partial x^2}\right)\right\rangle + \left\langle \frac{Eh}{(1-\nu^2)}\left(\frac{\partial v}{\partial y}+\nu\frac{\partial u}{\partial x}\right)\left(\frac{\partial v}{\partial y}-z\frac{\partial^2 w}{\partial y^2}\right)\right\rangle + \left\langle \left(\frac{1}{2(1+\nu)}\right)\left(\frac{Eh}{(1-\nu^2)}\right)\left(\frac{\partial v}{\partial x}+\nu\frac{\partial u}{\partial y}\right)\left(\frac{\partial u}{\partial y}+\frac{\partial v}{\partial x}-2z\frac{\partial^2 w}{\partial x\partial y}\right)\right\rangle \right\} dA \quad \ldots\ldots (59)$$

For external Hydraulic force of P_Z, external work per unit area of the bucket is given by:

$$\frac{dW_{ext}}{dA} = \sum \frac{1}{2} P_z w$$

$$W_{ex} = \frac{1}{2}\int_A (P_z w) dA \quad \ldots\ldots (60)$$

Substituting P_z from equation (48), it results:

$$W_{ex} = \frac{1}{2}\int_A \left(D\nabla^4 w\right)(w)\, dA \quad \ldots\ldots (61)$$

Where, $\nabla^4 w \equiv \frac{\partial^4 w}{\partial x^4} + 2\frac{\partial^4 w}{\partial x^2 \partial y^2} + \frac{\partial^4 w}{\partial y^4}$

Finally, the total strain energy will be the sum of U_o and W_{ex}, which results:

$$U = \frac{1}{2}\int_A \left\{ \left\langle \frac{Eh}{(1-\nu^2)}\left(\frac{\partial u}{\partial x}+\nu\frac{\partial v}{\partial y}\right)\left(\frac{\partial u}{\partial x}-z\frac{\partial^2 w}{\partial x^2}\right)\right\rangle + \left\langle \frac{Eh}{(1-\nu^2)}\left(\frac{\partial v}{\partial y}+\nu\frac{\partial u}{\partial x}\right)\left(\frac{\partial v}{\partial y}-z\frac{\partial^2 w}{\partial y^2}\right)\right\rangle + \left\langle \left(\frac{1}{2(1+\nu)}\right)\left(\frac{Eh}{(1-\nu^2)}\right)\left(\frac{\partial v}{\partial x}+\nu\frac{\partial u}{\partial y}\right)\left(\frac{\partial u}{\partial y}+\frac{\partial v}{\partial x}-2z\frac{\partial^2 w}{\partial x\partial y}\right)\right\rangle - \left(D\nabla^4 w\right)(w) \right\} dA \quad \ldots (62)$$

Now, we have equations for kinetic and strain/potential energy. The equations of motion can be derived using Newton's Law of motions, Lagrange's Equation of motion and Hamilton's Principle [27]. Since it is simple and convenient to use, we shall derive the equation of motion using Hamilton's Principle.

The general expression for the Hamilton's Principle between two arbitrary time's t_1 and t_2 expressed as [27].

$$\delta\int_{t_1}^{t_2}(T-U)dt=0 \quad \text{..... (60)}$$

One can use the equivalent equation, eq(61) of Hamilton's Principle as follows:

$$\frac{d}{dt}\left(\frac{\partial L}{\partial \dot{q}}\right)-\left(\frac{\partial L}{\partial q}\right)=0 \quad \text{..... (61)}$$

Where, the **Lagrangian L is** then a function of both the coordinates and their velocities.

$$L=T-U$$

Where T is the kinetic energy and U is the total strain potential energy of the bucket. Substituting the values of T and U in equation (61) results,

For X- Axis:

$$\left\langle \frac{d}{dt}\left[\tfrac{1}{2}\rho h\int_A\left\{2\left(\frac{\partial u}{\partial t}\right)+4\left(\frac{\partial u}{\partial t}\right)\left(u^2+v^2+w^2+u(v-w)+v(w+1)+w\right)-2\left(\frac{\partial v}{\partial t}\right)(u-w)-\left(\frac{\partial w}{\partial t}\right)(u+v)\right\}dA\right]\right.$$
$$-\left[\left\{\tfrac{1}{2}\rho h\int_A\left(2\left(\frac{\partial u}{\partial t}\right)^2(2u+v-w)-2\left(\frac{\partial u}{\partial t}\right)\left(\frac{\partial v}{\partial t}\right)-2\left(\frac{\partial u}{\partial t}\right)\left(\frac{\partial w}{\partial t}\right)\right)dA\right\}\right. \quad \text{..... (62)}$$
$$\left.\left.-\left\{\tfrac{1}{2}\int_A\left(\frac{Eh}{1-\upsilon^2}\right)\left(\frac{\partial^2 u}{\partial x^2}\right)dA\right\}\right]\right\rangle=0$$

For Y- Axis:

$$\left\langle \frac{d}{dt}\left[\tfrac{1}{2}\rho h\int_A \left(2\left(\frac{\partial v}{\partial t}\right) - 2\left(\frac{\partial u}{\partial t}\right)(u-w) \right) dA \right] - \left[\left\{ \tfrac{1}{2}\rho h\int_A \left(2\left(\frac{\partial u}{\partial t}\right)^2 (u+2v+w+1) - 2\left(\frac{\partial u}{\partial t}\right)\left(\frac{\partial w}{\partial t}\right) \right) dA \right\} - \left\{ \tfrac{1}{2}\int_A \left(\frac{Eh}{1-\upsilon^2}\right)\left(\frac{\partial^2 v}{\partial y^2}\right) dA \right\} \right] \right\rangle = 0 \quad \ldots(63)$$

For Z- Axis:

$$\left\langle \frac{d}{dt}\left[\tfrac{1}{2}\rho h\int_A \left(2\left(\frac{\partial w}{\partial t}\right) - 2\left(\frac{\partial u}{\partial t}\right)(u+v) \right) dA \right] - \left[\left\{ \tfrac{1}{2}\rho h\int_A \left(2\left(\frac{\partial u}{\partial t}\right)^2 (-u+v+2w+1) + 2\left(\frac{\partial u}{\partial t}\right)\left(\frac{\partial v}{\partial t}\right) \right) dA \right\} \right] \right\rangle = 0 \quad \ldots(64)$$

The boundary conditions can be taken from a Cantilever beam with a concentrated load at the middle assuming that the water jet force will be concentrated at the center of its diameter. The boundary conditions are:

At x=0, $u = o\ , v = o\ and, w = o$

Force and Moment, $M_{AB} = F_{Jet}(x-a)\ , M_{BC} = 0$

3.7 Rotating Pelton Turbine Bucket with a Crack

Due to crack formation, energy will be released. Thus, the total strain energy for the rotating bucket with a crack will be equal to total strain energy of the bucket without a crack minus the energy released due to crack formation.

$$U_T = U - U_C \quad \ldots\ldots \ldots\ldots\ldots\ldots\ldots\ldots\ldots\ldots\ldots\ldots\ldots (65)$$

Where, U_T is total strain energy of a bucket with a crack.

U is strain energy of a bucket without a crack.

U_C is strain energy released due to crack formation on the bucket.

3.7.1 The Strain Energy due to Crack

As discussed in Chapter 2, the released energy due to crack formation was described using Griffith energy balance. J-integral was also used to describe the released energy by a path around a crack tip.

The J-integral equation in equation (13) can now be re expressed with an equivalent equation given by equation (66):

$$J = \int_{\Gamma} \left(U dy - T_i \frac{\partial u_i}{\partial x} dS \right) \quad \text{..... (66)}$$

Using an axisymmetric property at the crack tip the same as that of the global coordinate axis of the rotating turbine bucket (*x*,y) , Mode I of a crack as it seen in figure 18, its J-integral expression is given in equation (67), where *ds* = *dxd*y ,

$$J = \int_{\Gamma} \left(U dy - \left(\sigma_{xx} \frac{\partial u}{\partial x} + \sigma_{yy} \frac{\partial v}{\partial y} + \sigma_{xy} \frac{\partial u}{\partial x} \right) dx dy \right) \quad \text{..... (67)}$$

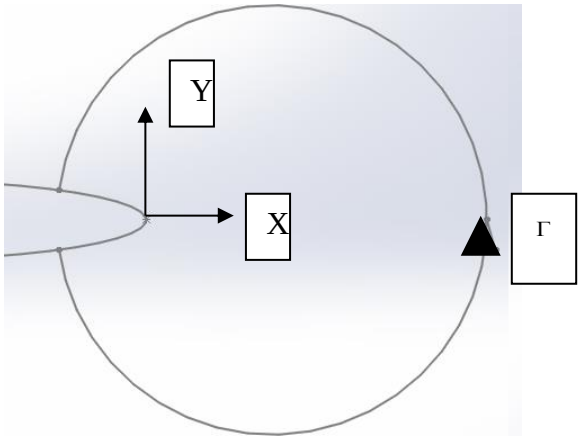

Figure 18: Integration path around crack tip

The loss of potential/strain energy due to crack formation on the bucket can be obtained by substituting equation (67) in equation (11):

$$-\frac{dE_p}{dA}=\int_{\Gamma}\left(Udy-\left(\sigma_{xx}\frac{\partial u}{\partial x}+\sigma_{yy}\frac{\partial v}{\partial y}+\sigma_{xy}\frac{\partial u}{\partial x}\right)dxdy\right) \quad \text{..... (68)}$$

Where, $E_p = U_C$ and A= A_C is area of crack.

Equation (68) can now be simplified and reduced to the following form.

$$\frac{U_C}{dA}=-\int_{\Gamma}\left(Udy-\left(\sigma_{xx}\frac{\partial u}{\partial x}+\sigma_{yy}\frac{\partial v}{\partial y}+\sigma_{xy}\frac{\partial u}{\partial x}\right)dxdy\right) \quad \text{..... (69)}$$

Equation (69) is a governing equation for fatigue crack propagation at the fixed end of the bucket. For each crack growth, the energy lost is quantified by equation (69). The life estimation of the crack can now be related with the J-Integral by assuming plain strain condition. Equation (69) can now be rewritten as:

$$U_C = J = -\int_{A_c}\left[\int_{\Gamma}\left(Udy-\left(\sigma_{xx}\frac{\partial u}{\partial x}+\sigma_{yy}\frac{\partial v}{\partial y}+\sigma_{xy}\frac{\partial u}{\partial x}\right)dxdy\right)\right]dA$$

The relation between energy release rate and stress intensity factor (K) with mode I fracture is given by:

$$J=\frac{1-\upsilon^2}{E}\Delta K_I{}^2 \quad \text{..... (70)}$$

Where, E is modulus of elasticity of the material and υ is the poisson's ratio

The above relation of equation (70) is to find the energy release rate from stress intensity factor if we wanted to calculate analytically. But in Ansys Workbench software, if we could specify the required inputs for fracture analysis; along with J value a value of K_I (stress intensity factor) can be obtained without further step. Once we could find the stress intensity factor (K_I), the fatigue life with increment of the crack depth can be estimated using Paris's law as discussed in chapter two in equation (6).

$$N = \int \frac{da}{C(\Delta K_I)^m}$$

Where, N is the fatigue life, da is increment in crack depth, C is constant and m is slop on the log-log plot.

For a given crack depth and applied stress, the stress intensity factor is given by:

$$K_I = \sigma Y \sqrt{a} \quad \ldots\ldots \quad (71)$$

Where, Y is a geometric factor which has a value of $Y = 1.12\sqrt{\pi}$ edge cracked specimen

The Stress σ is the applied water jet over the area of the bucket. Or simply, it is the applied pressure which can be obtained from the power input of the water jet.

The material property of Aluminum Alloy (**2024-T3**) is given by:

$$\sigma_{ulti} = 485MPa$$

$$K_{IC} = 44MPa\sqrt{m}$$

C= $2x10^{-9}$m/(MPa$\sqrt{m}$)$^{2.5}$/cycle, m=2.5 and the initial crack depth $a_o = 0.4mm$. K_{IC} is the fracture toughness of the material.

Using equation 72, the critical crack depth can be calculated from the following equation:

$$K_{IC} = \sigma_{\max} Y \sqrt{\pi a_c} \quad \ldots\ldots \quad (72)$$

$$a_c = \frac{1}{\pi} \frac{{K_{IC}}^2}{Y^2 {\sigma_{\max}}^2}$$

Here, the critical crack depth is a depth at which the fracture of the bucket happens. But also, the fracture is inevitable to happen when the crack depth enters the bolt hole as it is shown in figure 12. Therefore, the critical depth taken is 9.4mm.

From Paris law, the life of the bucket can be calculated using the following sets of equations.

$$\frac{da}{dN} = C\Delta K^m = C\left(Y\Delta\sigma\sqrt{\pi a}\right)^m$$

..... (73)

$$\int_0^{N_f} dN = \int_{a_i}^{a_f} \frac{da}{CY^m\Delta\sigma^m(\pi a)^{m/2}}$$

Equation (73) can be simplified and reduced to equation (74). Equation 74 is the equation which determines the life time of the bucket with a final crack a_f and a crack length a_i .

$$N_f = \frac{1}{CY^m\Delta\sigma^m\pi^{m/2}}\left[\frac{a_f^{1-\frac{m}{2}} - a_i^{1-\frac{m}{2}}}{1-\frac{m}{2}}\right] \quad \text{..... (74)}$$

Chapter Four

4 Finite Element Analyses

4.1 Introduction

The Finite Element Analysis (FEA) method is originally introduced by Turner et al. (1956. It is a computational technique for approximate solutions to different engineering problems having complex domains subjected to general boundary conditions [29].

ANSYS is the domain name commonly used for ANSYS mechanical, general-purpose finite element analysis (FEA) and computer aided engineering software tools developed by ANSYS Inc. ANSYS mechanical is analysis tool incorporating pre-processing such as modeling of geometry and meshing, solver and post processing modules in a graphical user interface.

The number of mesh determines the accuracy of the result and computational time. Increasing the number of mesh elements will increase the accuracy of the result and computational time and also it needs high performance computer. Decreasing the number of mesh elements will decrease the accuracy of the result and computational time. Thus to reduce such problems the usual trend is to use fine mesh in the area of interest (in this case the crack area) and course mesh away from the crack region.

Steps used in the solution procedure using ANSYS are the following:

- The geometry of the Pelton turbine bucket to be analyzed is imported in an IGS format.
- The materials properties of the bucket are specified.
- Meshing of the three-dimensional Pelton turbine bucket model is performed.
- The boundary conditions and external loads are applied.
- The solution is generated based on the previous input parameters.

4.2 Geometric Modeling of Pelton Turbine Bucket

Even though Ansys has a capability of modeling objects; due to the complexity of the shape of the bucket, Solid Works 16 have been used for modeling the three-dimensional model of the bucket. A Pelton turbine bucket without a crack is modeled as shown in figure 19 and 20. Where, the buckets and the disc of the runner are bolted together.

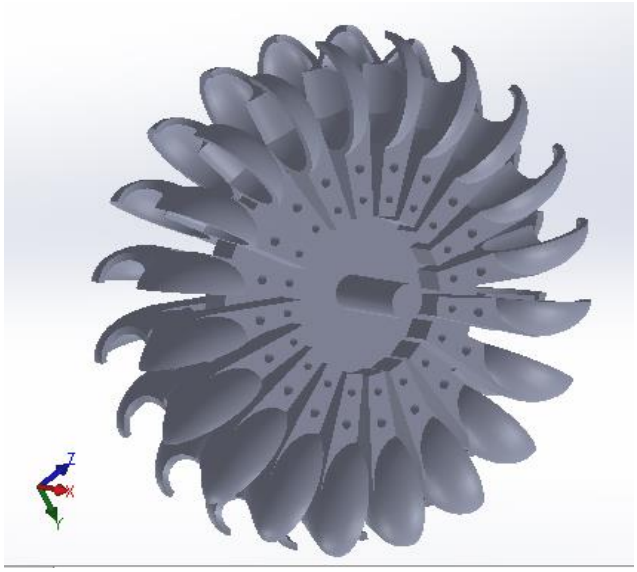

Figure 19. Pelton Turbine

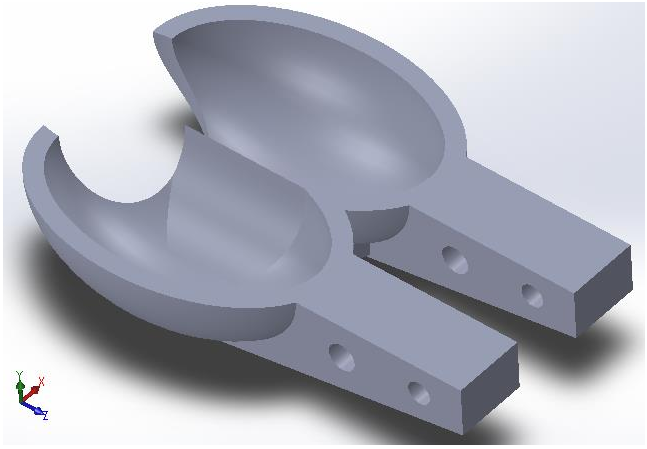

Figure 20. Pelton turbine bucket without a crack.

4.3 Defining of Material Properties

The selected material for Pelton turbine bucket is Aluminum Alloy (2024-T3) and the required properties for these analyses are given in Table 5.

Table 5. Material Properties of Aluminum Alloy (2024-T3)

σ_{Yild} (MPa)	$\sigma_{tens/comp}$ (MPa)	E (GPa)	υ	K_{IC} ($MPa\sqrt{m}$)	Density $\left(\frac{kg}{m^3}\right)$
345	485	73.1	0.33	44	2780

4.4 Generation of Mesh

The mesh with the default settings is not adequate to get the accurate results. In order to ensure accuracy of result, fine meshing for the tip of crack and global meshing for the remaining structure is performed. In this analysis the bucket around the crack area was finely meshed with "Sizing" option in menu. The element size for the region other than the crack surfaces was chosen to be 2mm. For regions near the elliptical crack surface a sphere of influence type is used in the sizing menu. The sphere radius is 20 mm and the element size is 0.5 mm. And a patch conforming algorithm was used to get a finer mesh. For fracture problems; as ANSYS 19.0 recommends, tetrahedral elements was used for region other than the crack surfaces and for fracture module Hexahedral mesh was used.

The number of elements in meshing affects the time and accuracy of analysis. A fine mesh results an accurate result but the time of analysis would be long. In order to get an accurate result with a medium period of time, half of the bucket is considered for the analysis by which the number of elements will be decreased and the analysis time is shortened.

It is shown in Table 6(a) that the whole body is selected and tetrahedron method is used. And in Table 6(b), the details of body sizing with the element size are shown. Having created a local coordinate system for crack location, a sphere of influence is used and a fined is used for regions near to the crack as it can be shown in Table(c). In figure 21, the bucket without a crack is meshed and the crack meh is shown in Figure 22.

Table 6. Details of Mesh in Ansys Workbench.

Details of "Patch Conforming Method" - Method	
Scope	
Scoping Method	Geometry Selection
Geometry	1 Body
Definition	
Suppressed	No
Method	Tetrahedrons
Algorithm	Patch Conforming
Element Order	Use Global Setting

(a)

Details of "Body Sizing" - Sizing	
Scope	
Scoping Method	Geometry Selection
Geometry	1 Body
Definition	
Suppressed	No
Type	Element Size
Element Size	2.e-003 m
Advanced	
Defeature Size	Default
Behavior	Soft

(b)

Details of "Body Sizing 2" - Sizing	
Scope	
Scoping Method	Geometry Selection
Geometry	1 Body
Definition	
Suppressed	No
Type	Sphere of Influence
Sphere Center	Coordinate System
Sphere Radius	2.e-002 m
Element Size	5.e-004 m

(c)

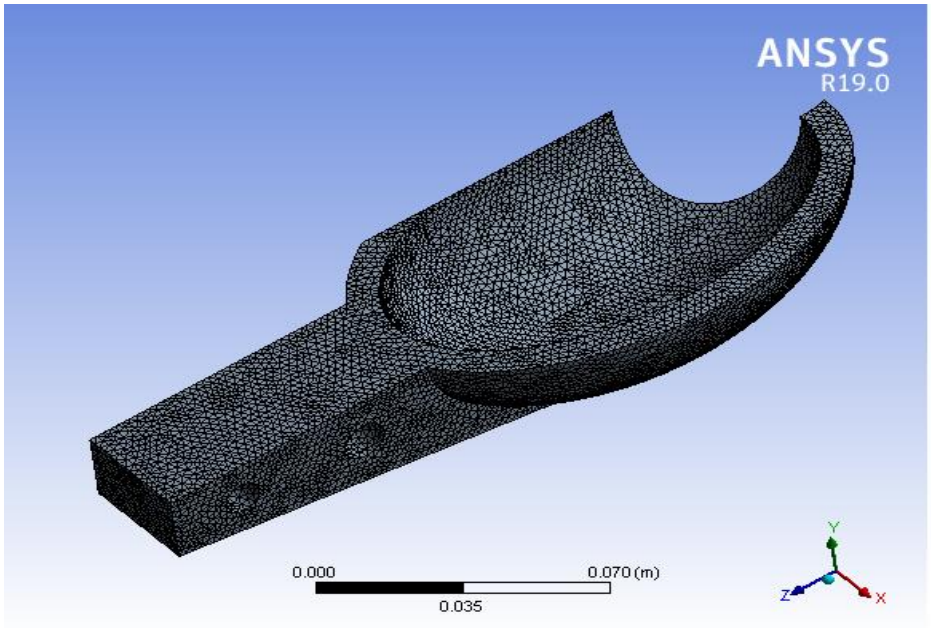

Figure 21. Meshed Bucket without crack

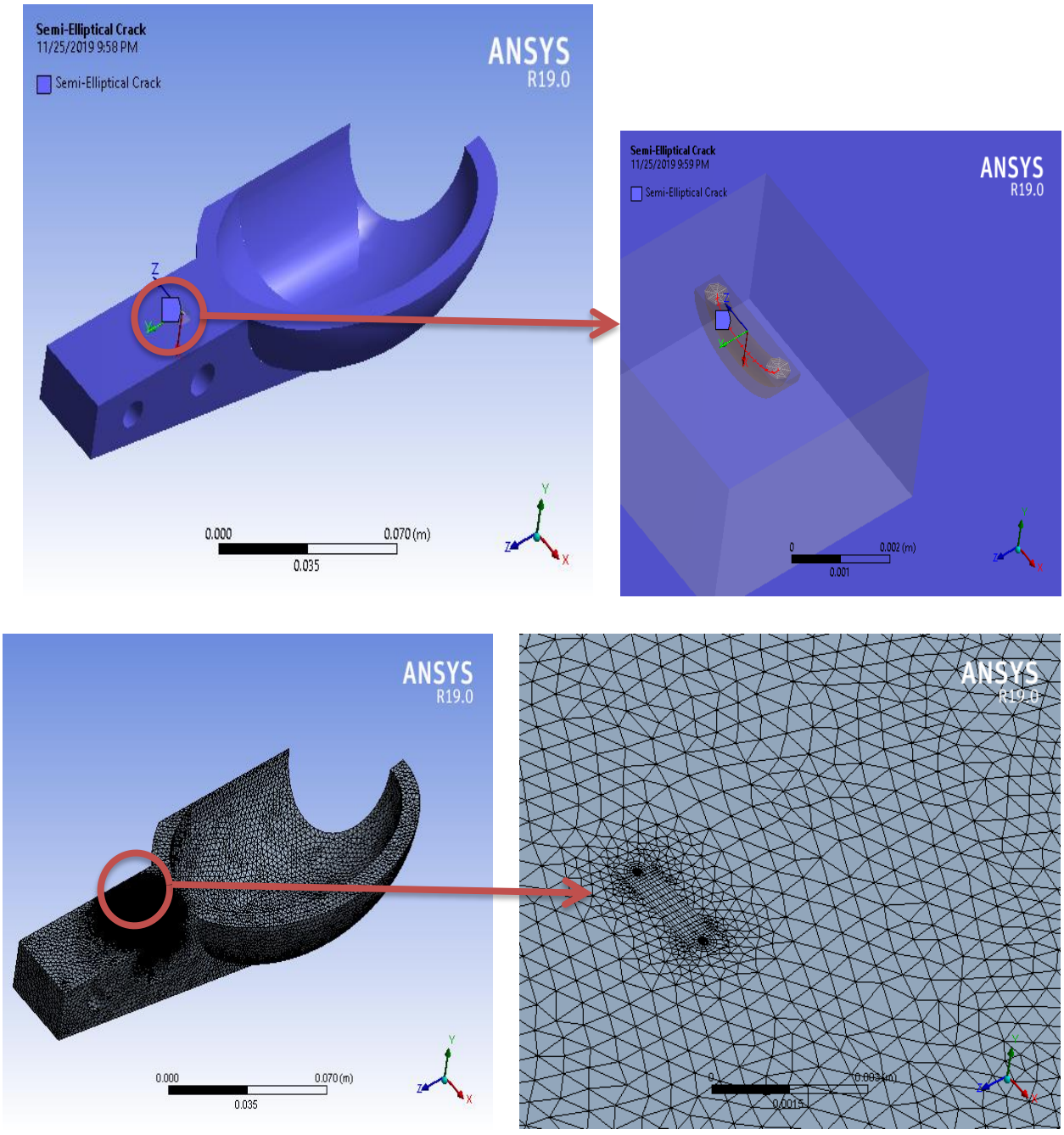

Figure 22. Meshed bucket around crack region

4.5 Boundary and Loading Conditions

As discussed earlier, considering the stem of bucket as a cantilever beam; one end of the bucket is fixed and the other is free, a water jet force on the area of impact is taken as a pressure with a value of 1.1901 MPa whenever the bucket interacts with the nozzle. The centrifugal force (angular velocity) of the bucket is also considered to be 195 rad/s with X-Axis as axis of rotation where this load is applied at each revolution which is shown in figure 23.

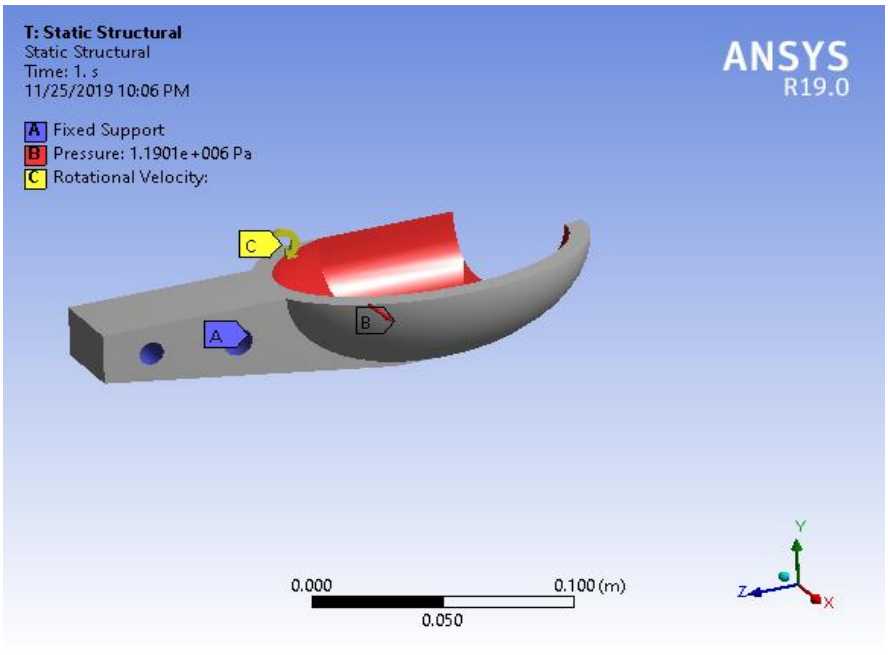

Figure 23. Boundary and Loading Conditions of Pelton turbine bucket

Chapter Five

5 Result and Discussion

Introduction

Considering only the lug (beam of the bucket), the stress profile can be given in figure 24.

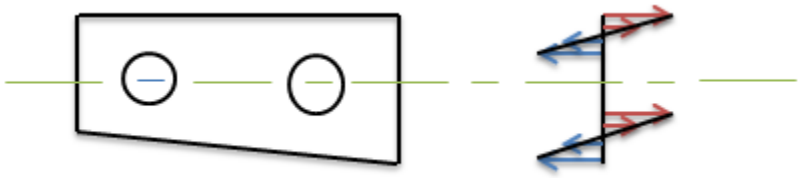

Figure 24: Stress profile of a bucket.

The red line represents the tensile regions and the blue line represents the compressive regions. But, it's a fact that a crack will propagate in a tensile region. Taking the upper top region of the bucket as a point of interest, a semi- elliptical crack was assumed to be initiated on the surface of stem. The initiated crack length (b) was taken to be 1mm and crack depth (a) of 0.4 mm. The nomenclature of the crack is given in figure 25.

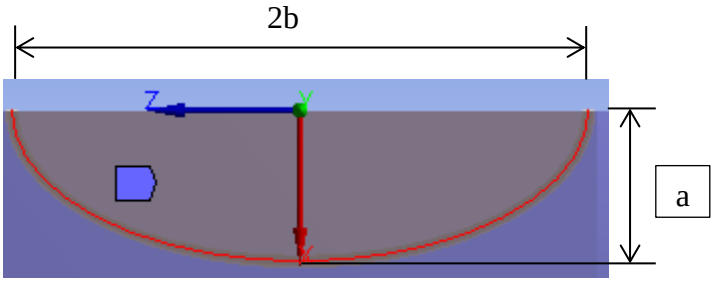

Figure 25: Crack Nomenclature

Using a crack aspect ratio (a/b), dimensions of the crack are calculated. As shown in Table 7, the crack aspect ratio and crack depth are related based on crack length. After b= 15.56, since it's the maximum crack length, the crack depth will increase 0.4 mm.

Table 7: Crack model summary

Crack Length, b (mm)	Crack Aspect Ratio(a/b)	Crack Depth, a (mm)
0	0.4	0
0.25	0.4	0.1
0.32175	0.4	0.1287
0.5	0.4	0.2
0.75	0.4	0.3
1	0.4	0.4
2	0.4	0.8
3	0.4	1.2
4	0.4	1.6
5	0.4	2
6	0.4	2.4
7	0.4	2.8
8	0.4	3.2
9	0.4	3.6
10	0.4	4
11	0.4	4.4
12	0.4	4.8
13	0.4	5.2
14	0.4	5.6
15	0.4	6
15.56	0.4113	6.4
15.565	0.43687	6.8
15.565	0.46257	7.2
15.565	0.48827	7.6
15.565	0.52039	8.1

The von-mises stress distribution of a bucket with crack is shown in figure 27. The maximum von-mises stress was located at the crack surface. This is because there is high stress concentration at the crack tip.

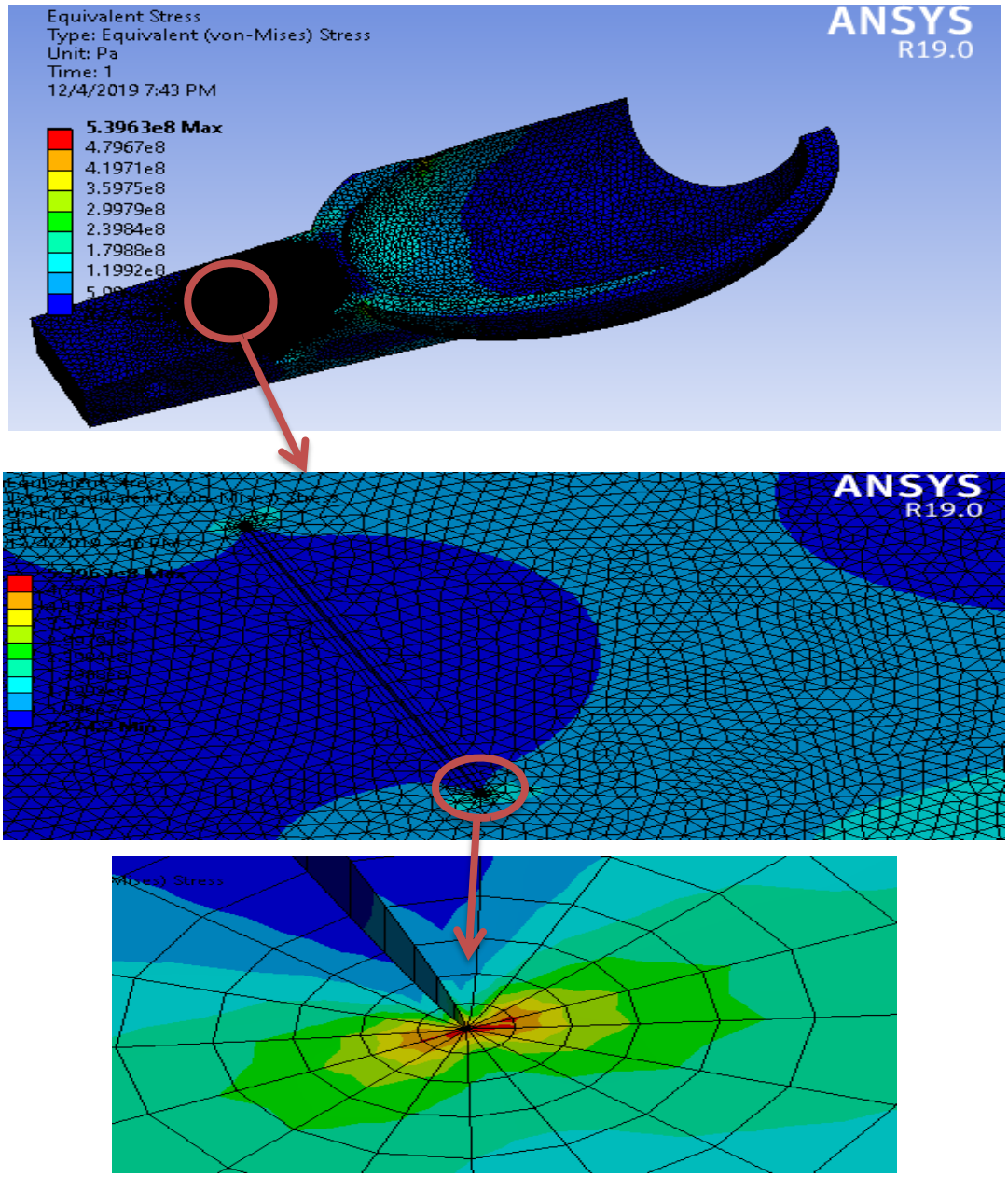

Figure 26:Von-mises stress distribution on the bucket for a=2.8mm

For each increment of crack depth, different fracture parameters are calculated and depicted in Table 8. Even though the critical crack depth is 9.4mm, the Ansys workbench fracture module could not read the value of crack depth above 8.1mm. Therefore, the analysis is done until 8.1 mm

of crack depth. However, the fracture of the bucket is inevitable to occur when the crack depth reaches 9.4mm.

Table 8: Different fracture parameters vs crack depth

Crack Depth, (a)(mm)	Crack Step	C	m	ΔK_I $\left(MPa\sqrt{m}\right)$	da/dN (m/cycle)	dN (cycles)	N (cycles)
0	0	0.000000002	2.5	0	5.7147E-09	0	0
0.1	1	0.000000002	2.5	1.5219	7.5362E-09	17499	17499
0.1287	2	0.000000002	2.5	1.7	1.3421E-08	17078	34576
0.2	3	0.000000002	2.5	2.1414	2.1870E-08	5313	39889
0.3	4	0.000000002	2.5	2.6033	3.0784E-08	4573	44461
0.4	5	0.000000002	2.5	2.9848	6.8275E-08	3248	47710
0.8	6	0.000000002	2.5	4.1048	1.0590E-07	5859	53569
1.2	7	0.000000002	2.5	4.8926	1.4191E-07	3777	57346
1.6	8	0.000000002	2.5	5.5004	1.7494E-07	2819	60165
2	9	0.000000002	2.5	5.9806	2.0560E-07	2286	62451
2.4	10	0.000000002	2.5	6.3796	2.3373E-07	1946	64397
2.8	11	0.000000002	2.5	6.7154	2.5929E-07	1711	66108
3.2	12	0.000000002	2.5	7.0001	2.8524E-07	1543	67651
3.6	13	0.000000002	2.5	7.2723	3.0796E-07	1402	69053
4	14	0.000000002	2.5	7.4987	3.2989E-07	1299	70352
4.4	15	0.000000002	2.5	7.7079	3.5710E-07	1213	71564
4.8	16	0.000000002	2.5	7.9562	3.8713E-07	1120	72685
5.2	17	0.000000002	2.5	8.2173	4.3494E-07	1033	73718
5.6	18	0.000000002	2.5	8.6091	5.8005E-07	920	74638
6	19	0.000000002	2.5	9.6599	8.9735E-07	690	75327
6.4	20	0.000000002	2.5	11.502	1.0321E-06	446	75773
6.8	21	0.000000002	2.5	12.164	1.2145E-06	388	76160
7.2	22	0.000000002	2.5	12.982	1.4936E-06	329	76490
8.1	23	0.000000002	2.5	14.102	5.7147E-09	268	76758

2.4 Stress Intensity Factor Solution

Stress intensity factor solutions for a three-dimensional crack has been computed and its solutions are shown in figure 27,28 and 29. For the initiated crack, the stress intensity factor along the crack front position shows that the three modes of fracture are available in the initiated semi elliptical crack. And as it can be seen in figure 27, the mode I stress intensity factor (K_I) is very large as compared with the other stress intensity factors (K_{II} and K_{III}). The maximum values of K_I, K_{II} and K_{III} are 2984800 Pa$\sqrt{m}$, 52159 Pa$\sqrt{m}$and 69677 Pa$\sqrt{m}$ respectively. From these values we can say that the fracture mode is mainly from opening mode.

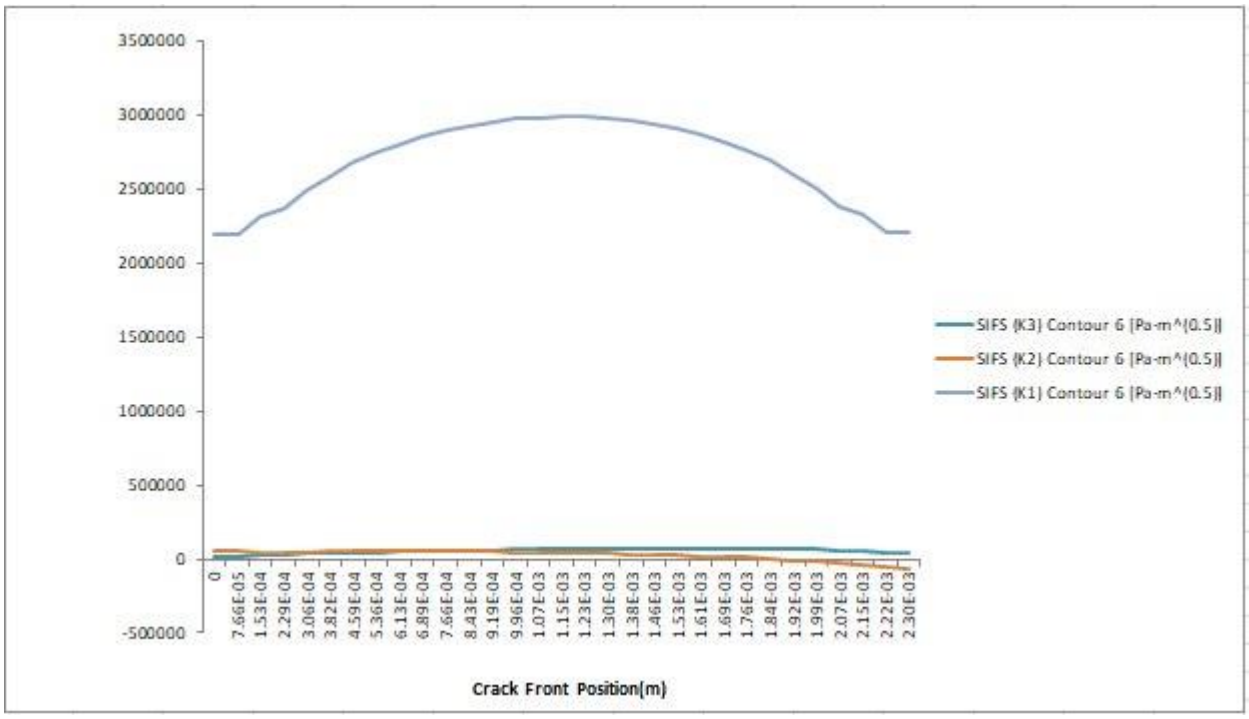

Figure 27: Stress intensity factors along crack front position

For each increment of crack length, stress intensity factors SIF are exported from Ansys 19 to Excel and ΔK1 was calculated by taking the difference between the maximum and minimum SIFs as depicted in table 8. Then with a crack depth, a curve was constructed for SIF.

It is shown in figure 28 that for an increase of crack depth and length, the SIF increases. The shape of SIF vs Crack depth graph is deviated from linearity. This is due to the fact that even

though it's assumed to neglect both KII and KIII, the crack is propagating in shearing and tearing mode too.

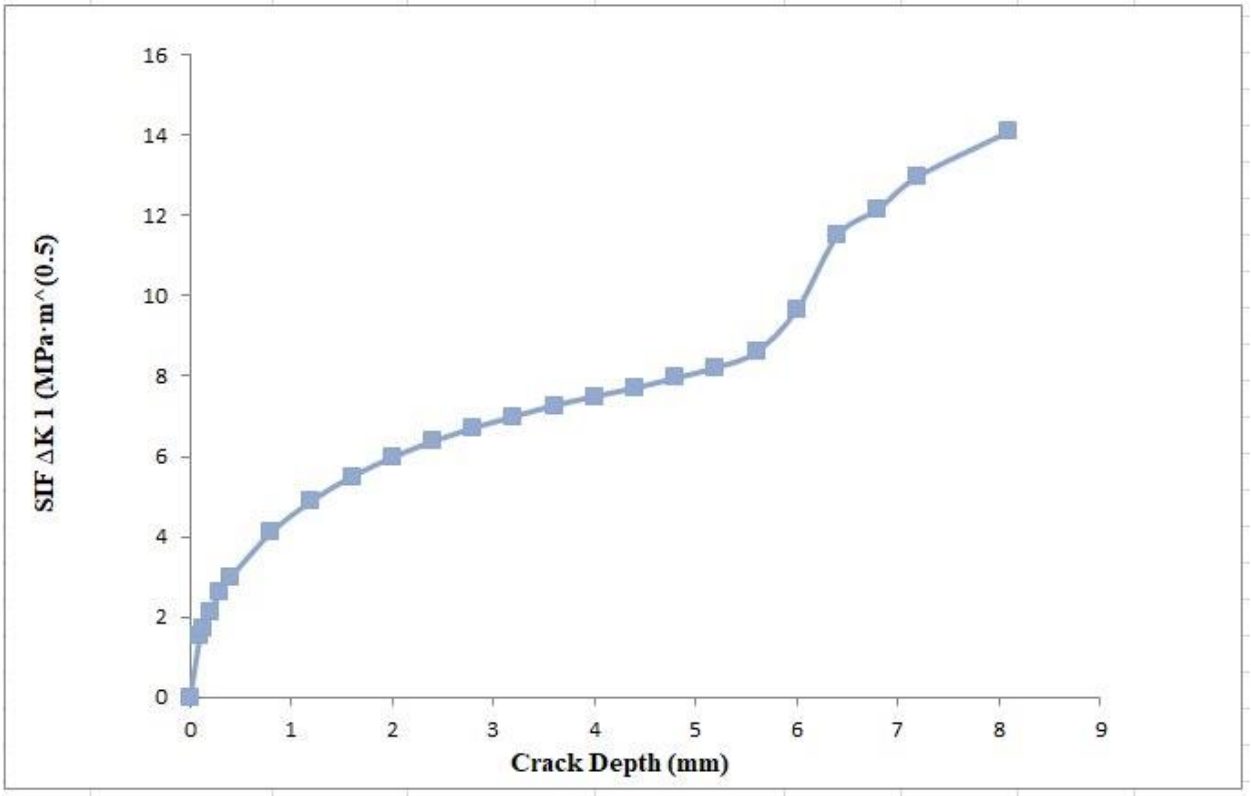

Figure 28: SIF K1 vs crack depth

2.5 Fatigue Crack Growth Rate and Fatigue Life

As discussed in chapter 2, the fatigue life is determined using Paris law which is applicable for region 2 of Figure 2. Having considered the material as elastic material, the constants C and m for Aluminum Alloy (2024-T3) alloy is interpolated using its strength property obtained to be the following values.

$$C= 2x10^{-9}\ m/(MP\sqrt{m})^{2.5}/cycle \text{ and } m=2.5$$

Using the above constants and geometric factor $Y = 1.12\sqrt{\pi a}$, the fatigue crack growth rate is calculated using Paris law equation as follows.

$$da/dN = C(\Delta K_I)^m$$

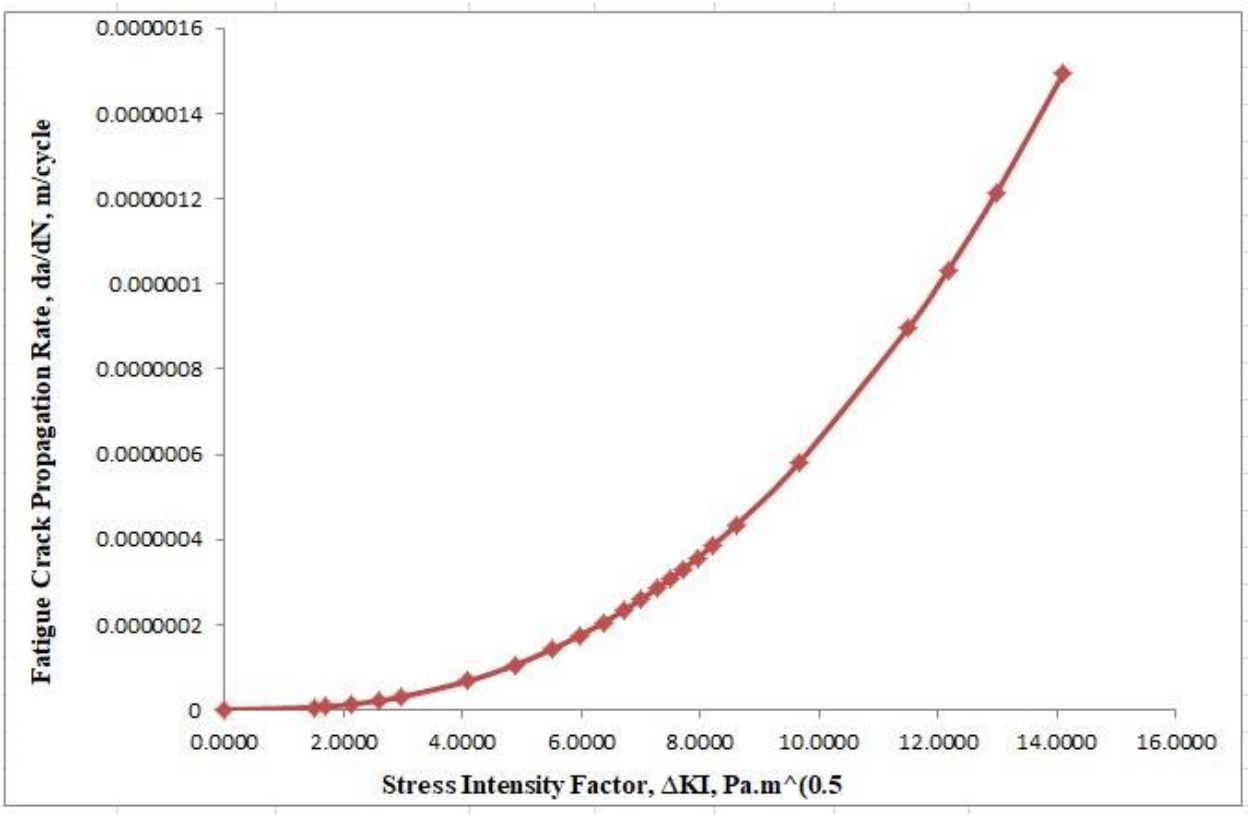

Figure 29: Fatigue crack propagation rate vs stress intensity factor

Figure 29 is the plot of fatigue crack growth rate and stress intensity factor, which illustrates typical fatigue crack growth behavior in Aluminum Alloy (2024-T3) alloy. It generally discusses the relationship in which for an increase in SIF, there is an increase in fatigue crack growth rate.

The curve contains region II and region III of Figure 2. At intermediate ΔK values, the curve is linear, but the crack propagation rate deviates from the linear trend at high and low ΔK levels. At the beginning of the curve since the level of ΔK is low, crack propagation rate approaches zero until the crack depth of 0.1287 mm. When the crack depth reaches 0.1287 mm, the ΔK levels become equal with the threshold value of stress intensity factor which 1.7 MPa$\sqrt{m}$. After this value the crack starts propagating and the rate increases nearly linearly until the crack depth is greater than 5.6mm.

At the crack depth of 5.6 mm, the crack propagates dynamically. Due to the influence of crack-tip plasticity on the true driving force for fatigue, the fatigue crack propagation rate increases rapidly until fracture happens, which is at a crack depth of 9.4 mm. Although the Paris equation is only valid for linear elastic fracture mechanics until the crack depth of 5.6mm, it is applied here with its limitations until the bucket is fractured.

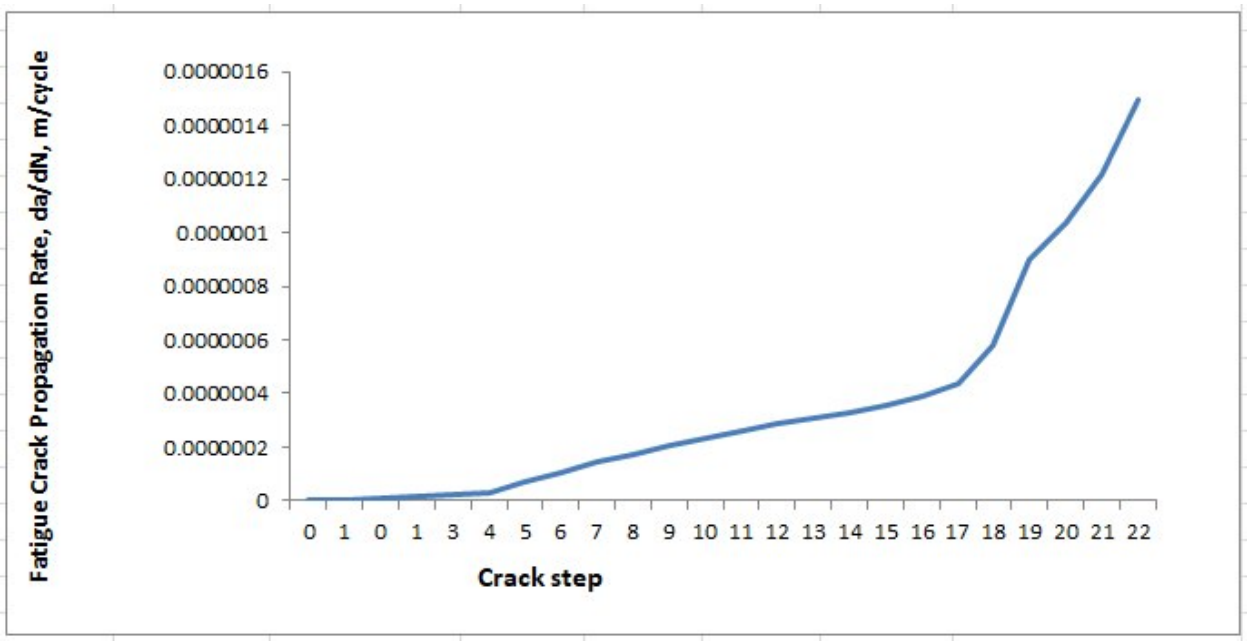

Figure 30: Fatigue crack propagation rate vs crack step

Figure 30 is the plot of fatigue crack growth rate and crack step. A crack step is a dimension less term given for the increment of crack depth. A crack step one refers to the crack depth has increased from 0mm to 0.1mm. The graph generally discusses the relationship on how fatigue crack growth rate increases when there is an increment of crack depth.

It can be shown in Figure 30 that fatigue crack propagation rate increases nearly linearly until a crack step of 18 (crack depth of 5.6 mm). After that it increases rapidly. This is due to the fact that at a crack depth of 6.8 the material crack propagation behaves become dynamic. After that the fatigue crack propagation rate increases rapidly until the point of fracture.

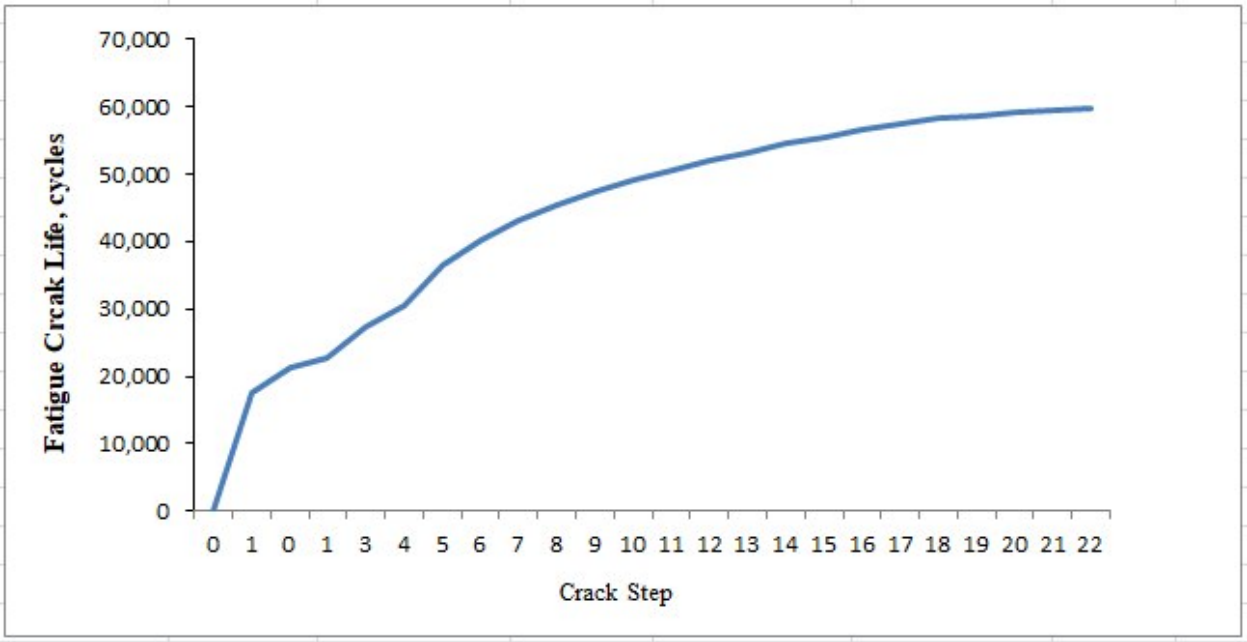

Figure 31: Fatigue Crack Life (cycles)

Using the stress intensity factor in Paris equation, fatigue crack growth rate was calculated and its values are tabulated in Table 8. As evident from figure 30, as crack depth increases Fatigue crack growth rate is found to be generally increasing. This means for each crack increment; the life of the bucket is shortened. The fatigue life of the bucket is then calculated for each crack depth increment and it's shown in figure 31.

Figure 31 shows the fracture fatigue cycles that the Pelton turbine bucket has been rotating with the increment of crack depth. For a crack step of zero, the reading fatigue crack life is 0 cycle. This means unless a crack is initiated a fatigue crack life is not determined. As the crack step increases the fatigue crack life increases to. For a crack step of 16 (crack depth of 4.8mm), the reading fatigue crack life is 2716670 cycles. This means, the bucket has been rotating 2716670 cycles until it reaches the plastic zone. Since the maximum crack depth analyzed is of 8.1 mm, one can read from figure 33 that the fatigue crack life of the Pelton turbine bucket is 2758440 cycles.

Chapter Five

6 Conclusion, Recommendation and Future work

6.1 Conclusion

In this thesis, the main objective is to analyze fatigue crack propagation and life estimation of Pelton turbine bucket. First a mathematical model which governs the propagation of the crack and its life estimation was derived. Having designed and geometrically modeled the bucket of Pelton turbine by Solidwork 2016, it was then imported to ANSYS Workbench 19.0. The boundary and loading condition of the bucket was then applied. Crack location in the bucket stem was identified from literature and fracture analysis for the operating conditions of Pelton turbine bucket was performed. From the results obtained, the following conclusions are drawn.

i. A governing equation derived in equations (62), (63) and (64) are equations of motions of a Pelton bucket and equation (69) can be used as a mathematical model for a fatigue crack propagation of Pelton turbine bucket.

ii. The von-mises stress increases with an increase of crack length as it is shown in figure 28. The increase of von-mises stress above the yield strength of material shows that there is a plastic deformation and as crack length increases, more damage is generated which leads to the failure of the bucket at a crack when the crack depth exceeds the geometry of the bucket, which is 9.4mm.

iii. Fatigue crack growth rate at each crack depth is determined and it was found that it increases with an increase in crack depth. Fatigue crack length propagation rate increased from $5.7147X10^{-6}$ to $1.4936X10^{-3}$ mm/cycle of crack length from 0.1 mm to 8.1 mm. The obtained solution is limited by contour integral evaluation for defined crack geometries and its orientation or crack propagation direction.

iv. When the crack depth reaches 8.1 mm, the fatigue crack life of the Pelton turbine bucket is 2758440 cycles.

From the results, I can conclude that the propagation of the crack is analyzed and the life estimation is performed for the obtained stress intensity factor.

6.2 Recommendation for Further Research

Fatigue crack growth rate at the crack depth increase with the increase in crack length. For more accurate solution, a method which takes care of all the three regions of Figure 3 under fatigue loading conditions should be considered.

In this thesis, only the effect of the applied water jet load and centrifugal force are taken into consideration. Other environmental loading conditions like: Vibrations of the bucket, corrosion, erosion problems, wear problems, cavitation, thermal load/ creep effect and effect of Surface finish of the material have not been addressed.

The applied stress exceeds the yield strength of the material prior to fracture. Even though linear elastic fracture mechanics has been applied, the truth shows there is a plastic fracture. I recommend future researchers to use both the elastic and plastic fracture mechanics approaches for analysis.

The effect of fatigue crack propagation will reduce the mechanical efficiency of the turbine. But, since it's not related mathematically, I recommend future researchers to study the effect of fatigue crack on efficiency of Pelton turbine.

Finally, it is recommended that experimental research can be performed for comparison of the numerical analysis result obtained. And, the effect of the above-mentioned loading conditions should be considered so that we could have a huge perspective to the fatigue crack propagation of the bucket.

7 References

[1]. Lejeune A, Hui SL. Hydropower: a multi benefit solution for renewable energy, 2012;6:15–47.

[2]. Hans-Jörg Huth, Fatigue Design of Hydraulic Turbine Runners, Doctoral thesis, 2005:19, ISBN 82-471-6899, February 2005.

[3]. Fatma Ayancik, Hydro-turbine Runner Design and Manufacturing, International Journal of Materials, Mechanics and Manufacturing, Vol. 1, No. 2, May 2013.

[4]. J.C. Chávez, J.A. Valencia, G.A. Jaramillo, J.J. Coronado, S.A. Rodríguez, Failure analysis of a Pelton impeller, 16 September 2014

[5]. https://images.search.yahoo.com/ Pelton Turbine Runner.

[6]. Ugyen Dorji and Reza Ghomashchi, Hydro turbine failure mechanisms: An overview, Engineering Failure Analysis 44 (2014) 136–147, 2 May 2014

[7]. Arne Kjølle, Hydropower In Norway, Norwegian University of Science and Technology, Trondheim, December 2001

[8]. Kværner Brug: COURSE III, Lecture compendium, Oslo 1986

[9]. Hydroplan UK, Low Cost Pelton Turbine Design and Testing,H/03/00074/REP,Gilbert Gilkes & Gordon Ltd. 2003

[10]. Gaur, P, Investigation of Fatigue Crack Propagation in Adhesively Bonded Joints used in Aluminum Vehicle Structures, July 2015

[11]. A.B. Winterbottom, Norges Tekniske Hogskole, Cracking of Bucket Lugs In Pelton Turbines a Corrosion Fatigue Phenomenon, Norway's Institute of Technology.

[12]. T. L. Anderson, Fracture Mechanics, 3ed, CRC Press LLC, 2005.

[13]. Reiner Mack, Pelton turbine design of Gilgel Gibe II, Voith Siemens Hydro's Product, May 2006

[14]. Sonendra, N. Agarwal and T.S.Deshmuk, Stress Analysis of Pelton Bucket Using

[15]. SIGMUND KYRRE ÅS, Fatigue Life Prediction of An Aluminum Alloy Automotive Component Using Finite Element Analysis of Surface Topography, Doctoral thesis 2006:25, ISBN 82-471-7790-0.

[16]. Bo Ernst Westergren Jensen, Numerical Analysis of Crack Propagation and Lifetime Estimation, Master Thesis, Aalborg University Esbjerg, June 2015.

[17]. Mulugeta Habtemariam, Fracture Analysis of Pressure Vessel under Dynamic Loading and Thermal Effect, Master thesis, Addis Ababa University, June, 2009

[18]. Meet Chapani and Bhairav Thakkar, Fatigue Life Estimation Of Low Cost Wind Turbine Blades Using Fracture Mechanics, ISSN 2319-8354, Apr 2016

[19]. Andrea Carpinteri, Camilla Ronchei, Daniela Scorza, Sabrina Vantadori, Fracture mechanics based approach to fatigue analysis of welded joints, Engineering Failure Analysis 49 (2015) 67–78, University of Parma, Parco Area delle Scienze 181/A, 43124 Parma, Italy.

[20]. M. Padhy and P. Senapati, Turbine Blade Materials Used for The Power Plants Exposed To High Silt Erosion, *ICHPSD-2015* , ITER, S'o'A University Bhubaneswar, Odisha, India.

[21]. J. Take, The Micro-Hydro Pelton Turbine Manual: Design, Manufacture and Installation for Small-Scale Hydro-Power, ITDG publishing, London, UK, 2000.

[22]. K.Chandra Sekhar and P.Venu Babu, Design and Analysis of Pelton Wheel Bucket, SISTAM College, JNTUK, India, ISSN No:2348-4845

[23]. Richard W. Hertzberg, Deformation and Fracture Mechanics of Engineering Materials, 4th Ed., ISBN 0-471-01214-9 (cloth), JOHN WILEY and SONS, INC.1996

[24]. Alexandre Perrig, Hydrodynamics of the Free Surface Flow in Pelton Turbine Buckets, *École Polytechnique Fédérale De Lausanne*, Thèse No 3715 (2007)

[25]. R.M. Rivello, Theory and Analysis of Flight Structures,", McGraw-Hill.

[26]. S.P. Timoshenko and S.Woinowsky-Krieger ,Theory of Plates and Shells,", McGraw Hill, 1951.

[27]. Donald T. Greenwood, Principles of Dynamics, University Of Michigan, Prentice-Hall, Inc. Englewood Cliffs, New Jersey, Isbn-10 0-511-07100-0 Eboo (Ebl), Cambridge University Press 2003.

[28]. E. J. Hearn, An Introduction to the Mechanics of Elastic and Plastic Deformation of Solids and Structural Materials, Third Edition, ISBN 0 7506 3266 6, 1997

[29]. Erdogan Madenci Ibrahim Guven, The Finite Element Method and Applications In Engineering Using Ansys, The University of Arizona, e-ISBN-13: 978-0387-282909, 2006.